HHS Public Access
Author manuscript
Cell Rep. Author manuscript; available in PMC 2022 September 22.

Published in final edited form as:
Cell Rep. 2022 August 02; 40(5): 111156. doi:10.1016/j.celrep.2022.111156.

METTL14-dependent m⁶A modification controls iNKT cell development and function

Liang Cao[1], **Eva Morgun**[1], **Samantha Genardi**[1], **Lavanya Visvabharathy**[1,3], **Yongyong Cui**[1], **Haochu Huang**[2,4], **Chyung-Ru Wang**[1,5,*]

[1]Department of Microbiology and Immunology, Feinberg School of Medicine, Northwestern University, 320 E. Superior Street, Searle 3-401, Chicago, IL 60611, USA

[2]Department of Medicine, University of Chicago, Chicago, IL 60637, USA

[3]Present address: Davee Department of Neurology, Feinberg School of Medicine, Northwestern University, Chicago, IL 60611, USA

[4]Present address: Department of Translational Oncology, Genentech, South San Francisco, CA 94080, USA

[5]Lead contact

Abstract

N^6-methyladenosine (m^{6}A), the most common form of RNA modification, controls CD4$^+$ T cell homeostasis by targeting the IL-7/STAT5/SOCS signaling pathways. The role of m^{6}A modification in unconventional T cell development remains unknown. Using mice with T cell-specific deletion of RNA methyltransferase METTL14 (T-*Mettl14*$^{-/-}$), we demonstrate that m^{6}A modification is indispensable for iNKT cell homeostasis. Loss of METTL14-dependent m^{6}A modification leads to the upregulation of apoptosis in double-positive thymocytes, which in turn decreases *Vα14-Jα18* gene rearrangements, resulting in drastic reduction of iNKT numbers in the thymus and periphery. Residual T-*Mettl14*$^{-/-}$ iNKT cells exhibit increased apoptosis, impaired maturation, and decreased responsiveness to IL-2/IL-15 and TCR stimulation. Furthermore, METTL14 knockdown in mature iNKT cells diminishes their cytokine production, correlating with increased *Cish* expression and decreased TCR signaling. Collectively, our study highlights a critical role for METTL14-dependent-m^{6}A modification in iNKT cell development and function.

Graphical abstract

*Correspondence: chyung-ru-wang@northwestern.edu.

AUTHOR CONTRIBUTIONS
L.C. and C.-R.W. conceived this study, designed the experiments, and analyzed the results. L.C., S.G., L.V., and Y.C. performed mice experiments. L.C. performed the cell culture experiments. E.M. analyzed sequencing data and constructed associated figures. H.H. provided critical reagent and expert advice. L.C., E.M., and C.-R.W. prepared the manuscript with comments from all authors.

SUPPLEMENTAL INFORMATION
Supplemental information can be found online at https://doi.org/10.1016/j.celrep.2022.111156.

DECLARATION OF INTERESTS
H.H. is an employee of Genentech.

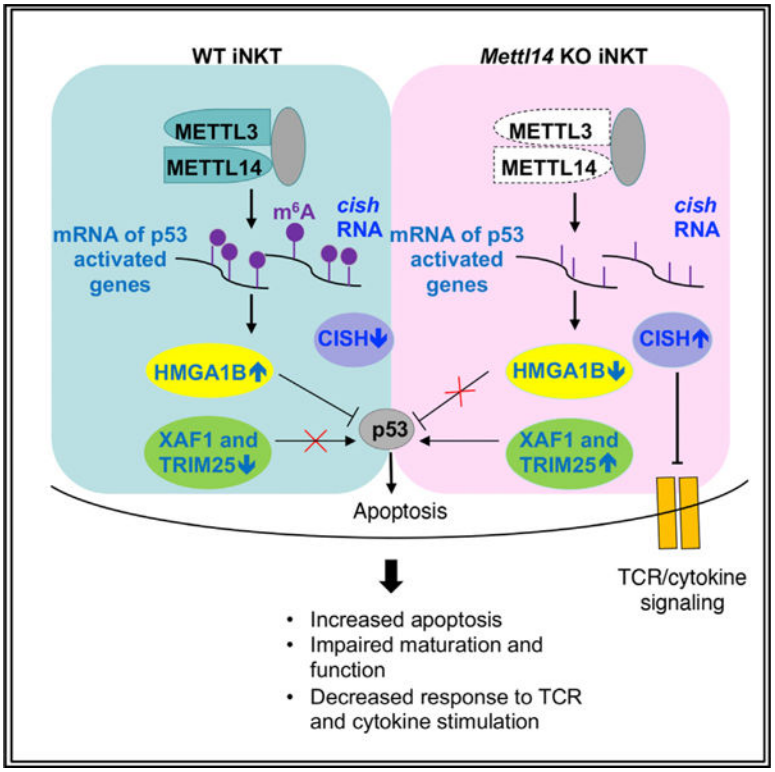

In brief

Cao et al. show that T cell-specific deletion of METTL14, a component of RNA m^{6}A writer complex, leads to severe defects in iNKT cell development, survival, and function. Mechanistically, METTL14-dependent m^{6}A modification controls iNKT cell development in a cell-intrinsic manner by regulating the apoptosis pathway and TCR signaling pathway.

INTRODUCTION

N^6-methyladenosine (m^{6}A) is the most abundant modification in eukaryotic mRNA (Bolger et al., 2014; Roundtree et al., 2017). m^{6}A modification influences mRNA splicing, stability, and translation efficiency (Meyer and Jaffrey, 2014; Roignant and Soller, 2017). It is also involved in long non-coding RNA (lncRNA)-mediated transcriptional repression (Shafik et al., 2016) and micro RNA genesis (Erson-Bensan and Begik, 2017). The machinery responsible for the dynamic deposition and recognition of m^{6}A on mRNA consists of ‘‘writers’’ that install m^{6}A modification on target RNAs, ‘‘reader’’ proteins that preferentially recognize m^{6}A and enact downstream functions, and ‘‘eraser’’ RNA demethylases that remove the m^{6}A modification (Fujii and Shimizu, 2019). The m^{6}A modification is mainly catalyzed by the m^{6}A writer complex composed of a methyltransferase-like (METTL) 3/METTL14 heterodimer and additional adaptor proteins (Ping et al., 2014). METTL3 contains the catalytic component and METTL14 binds and positions RNA for methylation and facilitates complex integrity (Liu et al., 2014).

The m^{6}A modification is involved in diverse cellular processes including cancer progression and metastasis (Lan et al., 2019), viral replication (Manners et al., 2019), stem cell differentiation (Batista et al., 2014), and embryonic development (Alarcon et al., 2015; Batista et al., 2014; Geula et al., 2015). Within the immune system, m^{6}A modification plays important roles in various immune cell types through the regulation of multiple signaling pathways. Previous studies with *Mettl3*$^{-/-}$ mice demonstrate that m^{6}A mRNA methylation controls CD4$^+$ T cell homeostasis by targeting the interleukin (IL)-7/STAT5/SOCS pathways (Li et al., 2017). METTL3-dependent m^{6}A modification is critical for T regulatory cell (Treg)-suppressive functions via IL-2/STAT5 signaling (Tong et al., 2018). Similarly, METTL14-deficient Treg cells fail to inhibit T cell-mediated colitis in mice (Lu et al., 2020). m^{6}A modification also controls early B cell development by regulating IL-7 signaling (Zheng et al., 2020). Mechanistically, the loss of m^{6}A modification results in slower mRNA decay and increased expression of the STAT signaling inhibitory proteins SOCS1, SOCS2, and CISH, which in turn inhibit cytokine-mediated STAT5 activation and therefore T cell proliferation and T cell differentiation. A recent study showed that METTL3-dependent m^{6}A modification also controls T follicular helper cell (T_{FH}) differentiation by regulating the expression of TCF-1, which in turn controls the expression of T_{FH} cell regulators, including BCL6, CXCR5, and ICOS (Yao et al., 2021). In addition, METTL3-mediated m^{6}A RNA modification promotes anti-tumor immunity of natural killer cells by maintaining SHP-2/IL-15/AKT pathway (Song et al., 2021). Despite all these advances, the role of m^{6}A modification in the development and function of unconventional T cells, including invariant NKT (iNKT) cells, remains unknown.

iNKT cells recognize self or foreign lipid antigens presented by CD1d, a non-classical major histocompatibility complex (MHC) class-I-like molecule (Kronenberg, 2005; Rossjohn et al., 2012). iNKT cells express semi-invariant T cell receptors (TCRs) formed by Vα14-Jα18 (Vα24-Jα18 in humans) TCRα-chain paired with Vβ8, Vβ7, and Vβ2 (Vβ11 in humans) (Bendelac et al., 2007). iNKT cells exhibit an effector-memory phenotype. Upon activation through TCR or cytokine signaling, iNKT cells rapidly produce a variety of cytokines, including interferon (IFN)-γ, IL-4, tumor necrosis factor, IL-17, and IL-10 (Crosby and Kronenberg, 2018). As innate-like lymphocytes, iNKT cells are mobilized as the first line of defense against cancers and infections (Juno et al., 2012; Slauenwhite and Johnston, 2015; Terabe and Berzofsky, 2018).

The developmental program of iNKT cells in the thymus diverges from conventional T cells at the double-positive (DP) stage. Unlike conventional T cells that are selected by MHC/peptide complexes on thymic epithelial cells, the positive selection of iNKT cells is mediated by CD1d-expressing DP thymocytes through homotypic interactions (Godfrey et al., 2010). iNKT cell development requires strong TCR signaling (Moran et al., 2011) to upregulate the expression of the transcription factor Egr2 (Lazarevic et al., 2009; Seiler et al., 2012) and PLZF (Kovalovsky et al., 2008; Savage et al., 2008), as well as signaling from the SLAM family receptors (Griewank et al., 2007; Sintes et al., 2013). Traditionally, iNKT cell development is divided into four stages: stage 0 (CD24^{hi}CD44$^-$NK1.1$^-$), stage 1 (CD24^{lo}CD44$^-$ NK1.1$^-$), stage 2 (CD24^{lo}CD44$^+$NK1.1$^-$), and stage 3 (CD24^{lo} CD44$^+$NK1.1$^+$) (Benlagha et al., 2005; Pellicci et al., 2002). iNKT cells can also be functionally classified into NKT1, NKT2, and NKT17 subsets based on the expression of transcriptional factors, T-bet, PLZF, GATA3, and RORγt (Constantinides and Bendelac, 2013; Lee et al., 2013). Recently, single-cell RNA sequencing (scRNA-seq) revealed comprehensive transcriptional profiles linked to the development, proliferation, maturation, and function of various iNKT cell subsets (Baranek et al., 2020; Engel et al., 2016). In addition, iNKT cells share overlapping developmental pathways, particularly with respect to cytokines, cell surface markers, and transcription factors needed for differentiation, with other innate T cell populations, including MAIT cells and γδ T cells (Harsha Krovi et al., 2020; Lee et al., 2020). This suggests that iNKT cells can serve as a useful model for understanding the development of unconventional T cells.

In this study, we used mice with a T cell-specific deletion of *Mettl14* (*Mettl14*$^{fl/fl}$*; CD4-Cre*$^{+}$, hereafter referred to as T-*Mettl14*$^{-/-}$) to investigate the role of m^{6}A modification on iNKT cell development and function. We found that loss of METTL14-dependent m^{6}A modification results in a dramatic decrease in the number of iNKT cells with a blockade of maturation occurring in a cell-autonomous manner. RNA-seq analysis of *Mettl14*$^{-/-}$ DP thymocytes revealed the abnormal expression of m^{6}A modified genes, such as *Hmga1b* and *Xaf1*, which could promote p53-mediated apoptosis. In addition, *Mettl14*$^{-/-}$ iNKT cells and *Mettl14*-knockdown (*Mettl14*^{KD}) mature iNKT cells had increased *Cish* expression, which attenuated TCR and cytokine signaling, leading to impaired cell proliferation and function. Of note, knocking down *Cish* expression in *Mettl14*^{KD} iNKT cell hybridomas restored their cytokine response. Collectively, our data demonstrate a critical role for METTL14-dependent m^{6}A modification in iNKT cell development, survival, and function.

RESULTS

m^{6}A is important for homeostasis of iNKT cells

As iNKT cells are innate-like T cells and have a different developmental program, they may harbor a different abundance in m^{6}A modification compared with conventional T cells. Interestingly, we found no significant differences in m^{6}A modification level among CD4$^+$, CD8$^+$ T cells, and iNKT cells. However, m^{6}A abundance was increased in iNKT cells after TCR stimulation (Figure 1A), indicating that m^{6}A modification may play a role in thymic selection and peripheral activation of iNKT cells. To understand the potential role of m^{6}A modification in iNKT development and function, we decided to use a loss-of-function mouse model. Previous work has shown that deletion of METTL14, a key component of the m^{6}A methyltransferase complex, abolished m^{6}A modification (Liu et al., 2014). Therefore, mice with a T cell-specific deletion of *Mettl14* (T-*Mettl14*$^{-/-}$) were used for this study to determine the role of METTL14 in iNKT development and function.

We first confirmed that the protein level of METTL14 was significantly reduced in both thymocytes and TCRβ$^+$ splenocytes from T-*Mettl14*$^{-/-}$ mice (Figure 1B). As METTL14 and METTL3 subunits are mutually required for protein stability (Kobayashi et al., 2018), the level of METTL3 protein was also decreased in both thymocytes and TCRβ$^+$ splenocytes from T-*Mettl14*$^{-/-}$ mice (Figure 1B). T cell-specific ablation of METTL14 resulted in a 2- to 3-fold reduction of total thymocytes; consequently, the absolute cell number of DP, CD4^{SP}, CD8^{SP}, and DN thymocytes in T-*Mettl14*$^{-/-}$ mice were substantially reduced compared with wild-type (WT) littermates (T-*Mettl14*$^{+/-}$) (Figure S1A). However, METTL14-deficiency had the most profound impact on iNKT cells; T-*Mettl14*$^{-/-}$ mice had an ~90% reduction in the percentage and cell number of iNKT cells in the thymus (Figures 1C–1E). Analysis of iNKT cells in the peripheral revealed that the percentage and absolute number of iNKT cells were also dramatically reduced (~5- to 10-fold) in the spleen and liver of T-*Mettl14*$^{-/-}$ mice as compared with WT littermates (Figures 1C–1E). In comparison, the total numbers of conventional CD4^{+} and CD8^{+} T cells were reduced by 2- to 3-fold in the spleen (Figure S1B). We also assessed the effect of METTL14-deletion on the development of other innate-like T cells, including CD1d-restricted type II NKT cells (defined as CD8^{-}NK1.1^{+}CD1d/PBS57 tetramer^{-} T cells) (Zhao et al., 2014) and MAIT cells, and found that the frequency and absolute number of both T cell types were significantly reduced in the thymus and liver of T-*Mettl14*$^{-/-}$ mice (Figures S1C–S1H). Thus, m^{6}A modification plays an important role in the development and homeostasis of innate-like T cells.

Impairment of iNKT cell homeostasis in T-*Mettl14*$^{-/-}$ mice is cell intrinsic

As iNKT cells were substantially reduced in T-*Mettl14*$^{-/-}$ mice, this led to the question of whether this deficiency was mediated by a cell-intrinsic or cell-extrinsic mechanism. We first assessed CD1d expression in DP thymocytes, the cell type responsible for positive selection of iNKT cells (Bendelac, 1995). CD1d expression was unaltered in T-*Mettl14*$^{-/-}$ DP thymocytes (Figure 2A). Similarly, the production of IL-2 was unchanged in the iNKT cell hybridoma DN32.D3 cocultured with WT or T-*Mettl14*$^{-/-}$ thymocytes pulsed with various concentrations of iNKT cell-specific ligand α-GalCer (Figure 2B), suggesting METTL14 deficiency does not affect the expression and antigen-presenting capacity of CD1d.

To determine whether METTL14 regulates iNKT cell development in a cell-intrinsic manner, we injected a 1:1 mixture of bone marrow cells (BM) from WT (CD45.1) and T-*Mettl14*$^{-/-}$ (CD45.2) mice into irradiated *Jα18*$^{-/-}$ mice lacking iNKT cells. We found that iNKT cells derived from T-*Mettl14*$^{-/-}$ BM only accounted for 2% to 5% of total reconstituted iNKT cells in the thymus, spleen, and liver of recipient mice (Figures 2C and 2D). Taken together, METTL14 deficiency affects iNKT cell development through a cell-intrinsic mechanism.

METTL14 deficiency impairs the maturation of iNKT cells

To further investigate the impact of m^{6}A modification on iNKT cell development, the maturation status of iNKT cells was analyzed in the thymus of T-*Mettl14*$^{-/-}$ mice. The percentages of iNKT cells from T-*Mettl14*$^{-/-}$ mice in stage 0–2 were increased compared with WT littermate controls, while the percentage of stage 3 iNKT cells was significantly decreased (Figures 3A and 3B). In terms of absolute cell numbers, all stages of iNKT cells in T-*Mettl14*$^{-/-}$ thymus decreased substantially except for those in stage 1 (Figure 3C). Interestingly, this developmental defect was not due to the lack of Egr2 (Figures S2A and S2B), a transcriptional factor that determines both early and late stages of iNKT lineage differentiation (Lazarevic et al., 2009; Seiler et al., 2012).

To further differentiate functional iNKT cell subsets, changes in the expression of three key transcription factors, PLZF, RORγt, and T-bet, were analyzed in thymic iNKT cells of

T-*Mettl14*$^{-/-}$ mice (Lee et al., 2013). The proportion of the RORγt^{+} NKT17 subset was not altered, but PLZF^{hi}RORγt^{-} iNKT cells, enriched for NKT2 and NKT cell precursors (NKT^{pre}) (Wang and Hogquist, 2018), were significantly increased and the T-bet^{+} NKT1 subset was significantly decreased in T-*Mettl14*$^{-/-}$ mice (Figures 3D and 3E). The absolute cell numbers of all three subsets were significantly decreased due to drastically lower iNKT cell numbers in T-*Mettl14*$^{-/-}$ mice (Figure 3F). These data showed that ablation of *Mettl14* results in impaired iNKT cell maturation and differentiation.

m^{6}A maintains DP thymocyte survival in part through regulation of the p53-mediated apoptosis pathway

In order to identify mechanisms by which METTL14 deficiency impaired iNKT cell development, DP thymocytes containing the precursor of iNKT cells from T-*Mettl14*$^{-/-}$ and littermate control mice were sorted for RNA-seq analysis. A total number of 117 differentially expressed genes (DEGs) were identified, of which 71 were protein-coding genes and 23 were long non-coding RNAs (lncRNAs) (Figures 4A and 4B). Interestingly, all differentially expressed lncRNAs were downregulated in the T-*Mettl14*$^{-/-}$ group, consistent with previous findings that m^{6}A modification stabilizes lncRNAs (He et al., 2020). Using gene set enrichment analysis (GSEA) (Subramanian et al., 2005), both p53 hallmark and apoptosis hallmark gene sets were positively enriched within the T-*Mettl14*$^{-/-}$ group with a normalized enrichment score of 0.99 and 0.93, respectively (Figures 4C, 4D, S3A, and S3B). Several potential key regulators of these pathways were identified within the DEG list. *Hmga1b*, one of the most significantly downregulated genes in *Mettl14*$^{-/-}$ DP thymocytes, encodes a chromatin-associated protein that is known to interact with p53 and inhibit its apoptotic function (Frasca et al., 2006). *Xaf1*, encoding a pro-apoptotic protein that can induce p53-mediated apoptosis (Lee et al., 2014), was upregulated in *Mettl14*$^{-/-}$ DP thymocytes. Another upregulated gene, *Trim25,* encodes an E3 ubiquitin ligase that controls the Keap1/Nrf2 pathway, known to promote survival of tumor cells (Liu et al., 2020) and increase the apoptosis of iNKT cells (Pyaram et al., 2019).

Using qPCR, we confirmed downregulation of *Mettl14* and *Hmga1b* and upregulation of *Trim25* and *Xaf1* in METTL14-deficient DP thymocytes (Figure 4E). To determine whether these genes may be direct targets of m^{6}A modification, m^{6}A-RNA-IP was performed using total RNA from B6 thymocytes in combination with cDNA generation/qPCR. *Hmga1b*, *Trim25*, and *Xaf1* were enriched within the m^{6}A-RNA-IP group, suggesting they are in fact direct targets of m^{6}A modification (Figure 4F).

Decreased *Hmga1b* and increased *Xaf1* expression suggest that activation of the p53-mediated apoptotic pathway may be enhanced in T-*Mettl14*$^{-/-}$ DP thymocytes. Indeed, higher percentages of Annexin V^{+} apoptotic cells were detected in *ex vivo*-isolated, *in vitro*-medium cultured, and anti-CD3/anti-CD4 stimulated T-*Mettl14*$^{-/-}$ DP thymocytes as compared with WT DP thymocytes (Figures 5A and 5B). As reactive oxygen species (ROS) are downstream mediators of p53-dependent apoptosis (Johnson et al., 1996), intracellular ROS between T-*Mettl14*$^{-/-}$ and WT DP thymocytes was compared using the cell-permeant florescent probe CM-H2DCFDA. ROS levels were elevated in T-*Mettl14*$^{-/-}$ DP thymocytes (Figure 5C), which correlated with increased apoptosis (Figure 5D). Interestingly, treatment with antioxidant N-acetyl-L-cysteine (NAC), a precursor of glutathione that is known to rescue thymocyte apoptosis by scavenging ROS (Pathak and Khandelwal, 2006) (Figure 5D), led to a decreased percentage of Annexin V^+ cells in T-*Mettl14*$^{-/-}$ DP thymocytes to a level comparable with WT DP thymocytes.

The enhanced level of apoptosis likely shortens the lifespan of T-*Mettl14*$^{-/-}$ DP thymocytes, which in turns reduces the efficiency of distal TCR recombination that iNKT cells harbor and therefore leads to an overall decreased number of thymic iNKT cells (Baldwin et al., 2004). Indeed, the mRNA level of *Vα14-Jα18* recombination, critical for the development of iNKT cells, was significantly decreased in $CD69^-$ preselection DP thymocytes isolated from T-*Mettl14*$^{-/-}$ mice (Figure 5E). We also evaluated whether the residual *Mettl14*$^{-/-}$ iNKT cells are more susceptible to apoptosis. iNKT cells in the thymus, spleen, and liver of T-*Mettl14*$^{-/-}$ mice had a higher percentage of Annexin V^+ cells. In addition, all stages of thymic iNKT cells in T-*Mettl14*$^{-/-}$ mice exhibited enhanced apoptosis (Figures 5F and 5G). These data suggest that disruption of METTL14-dependent m^6A modification results in altered expression of the key molecules involved in the p53-mediated apoptotic pathway, which may contribute to enhanced apoptosis of DP thymocytes and iNKT cells.

Upregulation of the m^6A target gene *Cish* in METTL14-deficient thymocytes correlates with decreased TCR signaling and impaired cytokine response

Absence of m^6A modification in T-*Mettl3*$^{-/-}$ mice resulted in elevated expression of several SOCS family genes, including *Socs1*, *Socs3*, and *Cish*, in $CD4^+$ T cells (Li et al., 2017). We explored whether SOCS family genes were also upregulated in T-*Mettl14*$^{-/-}$ DP thymocytes, which contain iNKT cell precursors. The expression of *Cish*, but not other SOCS family genes, was drastically increased in both naive and TCR-stimulated T-*Mettl14*$^{-/-}$ DP thymocytes, compared with their WT counterparts (Figures 6A and S4A). In addition, *Cish* was a direct target of m^6A modification in DP thymocytes (Figure 6B), similar to the finding in $CD4^+$ T cells (Li et al., 2017).

Cish is induced by TCR stimulation in T cells (Li et al., 2000) and plays an important role in regulating TCR and cytokine signaling (Matsumoto et al., 1997; Yoshimura et al., 1995) by targeting PLC-γ1 for proteasomal degradation (Palmer et al., 2015) and disrupting IL-stimulated STAT5 phosphorylation (Aman et al., 1999). To explore the functional consequence of Cish upregulation, we first evaluated the TCR-mediated calcium flux in DP thymocytes. T-*Mettl14*$^{-/-}$ DP thymocytes exhibited attenuated calcium influx compared with WT DP thymocytes both at TCR crosslinking and at Ca^{2+} addition stages (Figures 6C–6E). Next, we assessed the proliferative response of thymic iNKT cells to IL-2 or IL-15 stimulation (Gordy et al., 2011; Matsuda et al., 2002). While there was a 5-fold reduction in the percentage of iNKT cells in T-*Mettl14*$^{-/-}$ mice before stimulation, the differences widened after stimulation with IL-2 or IL-15, resulting in a 25-fold decrease in the percentage and 30-fold decrease in cell number of iNKT cells in T-*Mettl14*$^{-/-}$ mice (Figures 6F–6H). The diminished cytokine response in *Mettl14*$^{-/-}$ iNKT cells was further demonstrated by using cells labeled with CellTrace fluorescent dye (CFSE) to show that T-*Mettl14*$^{-/-}$ iNKT cells were less able to proliferate in response to IL-2 and IL-15 stimulation, compared with WT iNKT cells (Figure 6I). Moreover, phosphorylation of

STAT5, a downstream target in cytokine stimulation, was also decreased in IL-15-stimulated *Mettl14*$^{-/-}$ thymic iNKT cells (Figure 6J). These data suggest that elevated *Cish* expression due to the loss of m^{6}A modification may play a role in suppressing TCR and cytokine-mediated signaling in iNKT cells prior to egress into the periphery.

METTL14 deficiency impairs the function of mature iNKT cells

Having found METTL14-dependent m^{6}A modification is indispensable for thymic homeostasis and development of iNKT cells, next we addressed whether the function of peripheral iNKT cells in T-*Mettl14*$^{-/-}$ mice was affected. α-GalCer was injected into WT and T-*Mettl14*$^{-/-}$ mice to activate iNKT cells *in vivo* and IFN-g and IL-4 production by iNKT cells was evaluated using intracellular cytokine staining. We found that hepatic iNKT cells from α-GalCer-injected T-*Mettl14*$^{-/-}$ mice had a significantly lower percentage of IFN-γ and IL-4 single and double producing cells as compared with iNKT cells from α-GalCer-injected WT mice (Figures 7A and 7B). To determine whether METTL14-deficiency affects the expansion of iNKT cells *in vivo*, we evaluated iNKT cell proliferation and apoptosis on day 3 after α-GalCer injection. While the percentage of splenic iNKT cells increased approximately 20-fold in α-GalCer-injected WT mice, the percentage of iNKT cells in T-*Mettl14*$^{-/-}$ was only increased by 4-fold, compared with naive counterparts (Figures 1D, 1E, and S5A–S5C). In addition, splenic iNKT cells in α-GalCer-injected T-*Mettl14*$^{-/-}$ mice had a lower percentage of Ki67$^+$ and higher percentage of Annexin V$^+$ cells compared with WT control (Figures S5D and S5E). These results indicate that the function of residual iNKT cells is impaired in T-*Mettl14*$^{-/-}$ mice.

Since differentiation and maturation of iNKT cells is impaired in T-*Mettl14*$^{-/-}$ mice, the effect of METTL14-dependent m^{6}A modification on the function of mature iNKT cells was further assessed using the iNKT cell hybridoma DN32.D3 that stably expressed a short hairpin RNA (shRNA) targeting *Mettl14*. Two *Mettl14*-shRNAs were tested, but only sh2 was able to substantially knock down the expression of METTL14 in DN32.D3 cells (Figure 7C). In addition, m^{6}A modification level was significantly decreased in *Mettl14* knockdown (*Mettl14*^{KD}) DN32.D3 cells (Figure 7D). Knocking down *Mettl14* in DN32.D3 cells significantly increased the expression of *Cish* in both medium and α-GalCer stimulated conditions (Figure 7E), while other *Socs* family genes were slightly upregulated in the stimulated group (Figure S4B). In addition, production of IL-2 was significantly decreased in *Mettl14*^{KD} DN32.D3 cells after stimulation with α-GalCer (Figure 7F), which was consistent with their reduced calcium influx (Figures 7G–7H). To determine whether Cish upregulation contributed to the decreased TCR signaling and cytokine response in *Mettl14*^{KD} DN32.D3 cells, we knocked down *Cish* in *Mettl14*^{KD} DN32.D3 cells using retrovirus expressing shRNA targeting *Cish*. We found knocking down *Cish* in *Mettl14*^{KD} DN32.D3 cells (sh*Mettl14*-2/sh*Cish*) could restore IL-2 production to the level comparable to the control group (shNC/shNC) (Figures 7I and 7J).

The CRISPR-Cas9-mediated gene targeting method (Seki and Rutz, 2018) was also used to delete *Mettl14* in splenic iNKT cells from *Vα14*Tg mice. An ~70% reduction in *Mettl14* transcript level was observed in iNKT cells transfected with rCas9/gRNA-*Mettl14* complex as compared with iNKT cells transfected with negative control (NC) (Figure 7K). Consistent with the *Mettl14*^{KD} results in the iNKT hybridoma cell line (DN32.D3), the expression of *Cish* was also significantly increased in rCas9/gRNA-*Mettl14*-treated primary splenic iNKT cells (Figure 7K). In addition, the total number of iNKT cells was significantly decreased in the rCas9/gRNA-*Mettl4* treated group (Figure 7L). The percentage of IFN-γ-producing iNKT cells was also reduced in the rCas9/gRNA-*Mettl14*-treated group upon anti-CD3 stimulation (Figure 7M). These data suggested that METTL14-dependent m^{6}A modification affects the function of mature iNKT cells by regulating *Cish* expression.

DISCUSSION

In this study, we described the critical requirement for METTL14-dependent m^{6}A modifications in iNKT cell development and function. Our data suggest that the drastic reduction of iNKT cell population in T-*Mettl14*$^{-/-}$ mice is likely due to the enhanced apoptosis of DP thymocytes mediated by p53 apoptotic pathway activation and impaired responses to IL-2/IL-15 and TCR stimulation as a consequence of elevated *Cish* gene expression. Knocking down *Mettl14* in mature iNKT cells also leads to decreased TCR signaling and cytokine production, which is correlated with increased expression of *Cish*, as knocking down *Cish* expression restored the function of iNKT cells.

Previous study with T-*Mettl3*$^{-/-}$ mice showed that thymocyte populations did not change significantly in number or percentage (Li et al., 2017) but in T-*Mettl14*$^{-/-}$ mice, all thymocyte subsets were decreased in cell number, with particularly striking effects on iNKT cells (Figures 1C–1E, and S1A). CD4$^+$ T cells in T-*Mettl3*$^{-/-}$ mice did not show increased apoptosis after *ex vivo* culture. In contrast, T-*Mettl14*$^{-/-}$ mice had elevated apoptosis in both DP thymocytes (Figures 5A and 5B) and iNKT cells (Figures 5F and 5G) due to the upregulation of pro-apoptotic genes and downregulation of anti-apoptotic genes (Figure 4E). Furthermore, CD4$^+$ T cells in T-*Mettl3*$^{-/-}$ mice failed to expand upon stimulation with IL-7 because of elevated expression of several *SOCS* genes, including *Socs1*, *Socs3*, and *Cish*. *Cish* was the only upregulated gene in the SOCS family in T-*Mettl14*$^{-/-}$ DP thymocytes after stimulation (Figures 6A and S4A), leading to an attenuated response to cytokine and TCR stimulation (Figures 6C–6J). The differences observed in T-*Mettl3*$^{-/-}$ and T-*Mettl14*$^{-/-}$ mice could in part be due to incomplete deletion of *loxP* flanked genes during T cell development in these mouse models. In addition, recent studies have indicated that METTL3 can directly control the translation process of certain mRNA by recruiting eIF3 without the coordination with METTL14 in some human cancer cells (Choe et al., 2018; Lin et al., 2016). Further study is required to determine specific genes targeted by these two METTLs in the development and function of various T cell subsets.

GSEA analysis of RNA-seq results showed that the p53 pathway and apoptosis pathways were enhanced in T-*Mettl14*$^{-/-}$ DP thymocytes. Therefore, the apoptotic-related genes, such as *Hmga1b*, *Xaf1* and *Trim25*, were analyzed to confirm their mRNAs were m^{6}A targets (Figures 4E and 4F). Increased apoptosis was consistently observed in T-*Mettl14*$^{-/-}$ DP thymocytes in both naive and activated states (Figures 5A and 5B). While our data indicated that METTL14 regulates iNKT cell development mostly in a cell-intrinsic fashion (Figure 2), the relative overall reduction in DP thymocytes, which are critical for iNKT cell positive selection, may also contribute to the drastic reduction of iNKT cells in T-

Mettl14$^{-/-}$ mice. It has been shown that mature iNKT cells have a greatly increased ROS level compared with CD4^{+} and CD8^{+} T cells (Kim et al., 2017). In addition, iNKT cells are more susceptible to oxidative stress compared with conventional T cells (Kim et al., 2017). The elevated apoptosis in T-*Mettl14*$^{-/-}$ DP thymocytes was completely rescued by NAC treatment, indicating m^{6}A may control homeostasis of DP thymocytes by restraining p53-mediated apoptosis. Interestingly, deficiency of *Mettl3* also leads to enhanced apoptosis by modulating p53 signaling pathway in HepG2 cells (Dominissini et al., 2012) and the arsenite-transformed human keratinocytes (Zhao et al., 2020).

Other genes regulated by m^{6}A modification may be involved in the control of iNKT cell development and function, such as *c-myc*, *c-myb*, *Pten*, and *Bcl-2*. c-Myc, c-Myb, and PTEN are required for iNKT cell development and homeostasis (Dose et al., 2009; Hu et al., 2010; Kishimoto et al., 2007; Mycko et al., 2009) and BCL-2 is an anti-apoptotic molecule that maintains iNKT cell survival (Zhu et al., 2018). In addition, iNKT cell development and function require nuclear factor-κB signaling (Stanic et al., 2004), which is modulated by m^{6}A modification (Wang et al., 2019). However, none of these genes were differentially expressed in T-*Mettl14*$^{-/-}$ DP thymocytes compared with their WT counterparts based on RNA-seq data. Notably, the GSEA analysis revealed that *c*-Myc-target genes, which have been reported to maintain iNKT cell differentiation and function (Dose et al., 2009; Mycko et al., 2009), were significantly decreased (Figure S6A). In addition, Notch signaling, which has been shown to inhibit iNKT cell differentiation and function (Oh et al., 2015), was upregulated in T-*Mettl14*$^{-/-}$ DP thymocytes (Figure S6B). Therefore, m^{6}A modification may regulate iNKT cell development through multiple signaling pathways.

lncRNAs are a class of non-coding RNA transcripts that are longer than 200 base pairs and have metabolic and regulatory functions (Fernandes et al., 2019). m^{6}A modification increases the stability of lncRNA (He et al., 2020). The lncRNAs in T-*Mettl14*$^{-/-}$ DP were all downregulated due to the absence of the m^{6}A modification. One lncRNA, Gm15441, was shown to attenuate inflammasome activation in response to PPARα agonism and fasting (Brocker et al., 2020), which might explain the activation of pro-inflammatory pathways in our GSEA analysis (Figure S6C). However, little is known about the role of lncRNAs in NKT cell development and function, which warrants further investigation.

Alterations in m^{6}A patterns are associated with human diseases such as cancer initiation and progression. There is growing interest in developing m^{6}A writer-based strategies to combat cancer (He and He, 2021). Specifically, inhibitors targeting METTL3 catalytic function have been developed (Dolbois et al., 2021; Moroz-Omori et al., 2021) and have shown promise in the treatment of acute myeloid leukemia (Yankova et al., 2021). These inhibitors could potentially be useful to delineate the temporal requirement for m^{6}A modification in T cell development, homeostasis, and function. In this study, we demonstrated m^{6}A modification was critical for the development and function of iNKT cells through orchestrating the regulation of multiple genes involved in cell survival and TCR signaling. As iNKT cells are innate-like T cells playing important roles in autoimmune disease, infection, and tumor immunity (Bedard et al., 2017; Fujii and Shimizu, 2019; Galvez et al., 2021; Van Kaer and Wu, 2018), clinical application of targeting m^{6}A methyltransferases should consider the impact on the homeostasis and function of iNKT cells and the benefits to the treatment of chronic disease.

Limitations of the study

In this study, we showed that genes involved in several signaling pathways are differentially regulated in *Mettl14*-deficient DP thymocytes, including pathways associated with c-Myc, Notch, and inflammation. However, we have not directly investigated the impact of these pathways on iNKT cell development and function in T-*Mettl14*$^{-/-}$ mice. Furthermore, due to the very limited number of residual thymic iNKT cells in T-*Mettl14*$^{-/-}$ mice, we used total thymocytes instead of purified iNKT cells in most *in vitro* assays, and therefore cannot exclude the possibility that other cell types may affect iNKT cell responses in these experiments. Finally, since *Mettl14* was deleted in all the CD4 expressing populations, some of the observed phenotypic changes in iNKT cells may be due to changes in their interactions with other T cells.

STAR☆METHODS

RESOURCE AVAILABILITY

Lead contact—Further information and requests for resources and reagents should be directed to and will be fulfilled by the lead contact, Chyung-Ru Wang (chyung-ru-wang@northwestern.edu).

Materials availability—This study did not generate new unique reagents.

Data and code availability—The accession number of RNAseq data for DP is GSE189339 in NCBI (https://www.ncbi.nlm.nih.gov/geo/query/acc.cgi?acc=GSE189339).

Scripts used for alignment and counting can be found here (https://github.com/ebartom/NGSbartom). Downstream analysis was performed as described in method details.

Any additional information required to reanalyze the data reported in this paper is available from the lead contact upon request.

EXPERIMENTAL MODEL AND SUBJECT DETAILS

Mice—C57BL/6 (B6), *Vα14-Jα18* transgenic (*Vα14*Tg) mice and CD45.1 congenic B6 mice were purchased from The Jackson Laboratory. *Mettl14*$^{fl/fl}$*; CD4-Cre*$^{+}$ mice have been described previously (Lu et al., 2020) and were backcrossed for 10 generations onto B6 background. Littermates were used as controls. *Jα18*$^{-/-}$ mice on the B6 background were kindly provided by Dr. Luc Van Kaer (Vanderbilt University). All mice for each experiment were sacrificed between 2–4 months of age. Both males and females were used. All mouse experiments were approved by the institutional animal care and use committee (IACUC) at Northwestern University. All animals were housed in a specific-pathogen-free facility according to institutional guidelines.

Cell culture and *E. coli* culture—Splenocytes from *Vα14*Tg mice were stimulated with plate-bound anti-CD3 (5 μg/mL) and soluble anti-CD28 (2 μg/mL) for 24 h and subjected to nucleofection. Then the splenocytes were maintained in complete RPMI supplemented with 10% FBS, 2 mM Glutamine, 10 mM HEPES, 55 μM 2-ME, 100 units/mL penicillin and 100 μg/mL streptomycin in the presence of IL-2 (200 U/mL) in 5% CO_2 incubator at 37°C. Thymocytes were labeled with CellTrace™ CFSE (Invitrogen) according to the manufacture's protocol and cultured in the presence of IL-2 (200 U/mL) or IL-15 (100 ng/mL). iNKT hybridoma (DN32.D3) cells, 293T cells and Phoenix-Eco cells were maintained in DMEM supplemented with 10% FBS, 10 mM HEPES, 100 units/mL penicillin and 100 μg/mL streptomycin or additional 5 ug/mL puromycin for selecting stably transduced DN32.D3 hybridoma cell line. Stbl3™ *E. coli* was cultured in LB medium at 37°C with vigorous agitation.

METHOD DETAILS

T cell enrichment, stimulation, RNA extraction and m^{6}A quantification—CD4$^+$ and CD8$^+$ T cells from B6 mice were enriched with anti-CD4 (L3T4) and anti-CD8α (Ly-2) MicroBeads (Miltenyi Biotec), respectively. iNKT cells were enriched from *Vα14*Tg mice by negative selection with biotinylated antibody specific to B220 (RA3–6B2), CD19 (6D5), CD8α (53–6.7), CD8β (53–5.8), CD11b (M1/70), CD11c (N418), Ter119 (TER-119), and I-A/I-E (M5/114.15.2) in combination with Dynabeads™ Biotin Binder (Invitrogen) followed by staining of iNKT cells for cell sorting (resting and *in vivo* activated). Total RNA was isolated from purified CD4$^+$, CD8$^+$ and iNKT cells with Qiagen RNAeasy® mini kit and subjected to mRNA enrichment (Mathur et al., 2021). mRNA concentration was quantified by Qubit™ RNA High Sensitivity (Thermo Fisher). Quantification of m^{6}A in total mRNA was performed based on the protocol of manufacture by enzyme-linked immunosorbent assay (ELISA) (EPIGENTEK) (Song et al., 2021).

Immunoblotting—Total thymocytes, sorted TCRβ$^+$ splenocytes and DN32.D3 cells were lysed in RIPA buffer and immunoblotting was performed using polyclonal antibody against METTL14 (Sigma) and METTL3 (Proteintech). Anti-α-tubulin (DM1A, Calbiochem) was used as a loading control according to the protocol described previously (Sena et al., 2013).

Antibodies and flow cytometry—Fluorescein isothiocynate (FITC)-conjugated anti-CD1d (5C6) was generated in our lab (Mandal et al., 1998). PE and Allophycocyanin (APC)-conjugated PBS57/mCD1d-tetramer, mCD1d unloaded tetramer, 5-OP-RU and 6-FP-loaded MR1 tetramers were obtained from the NIH tetramer core facility. Single cell suspensions from various organs were prepared and stained as described previously (Goossens et al., 1990; Zimmer et al., 2006). Cells were stained with the following surface markers: anti-TCRβ (H57–597), anti-CD8*α* (53–6.7), anti-CD4 (RM4–5), anti-NK1.1 (PK136), anti-CD24 (M1/69), anti-CD44 (IM7) anti-F4/80 (BM8), anti-CD69 (H1.2F3), anti-B220 (RA3–6B2), anti-CD45.1 (A20), anti-CD45.2 (104), anti-EGR2 (erongr2) and Annexin V/7AAD. Intracellular staining of anti-PLZF (9E12), anti-T-bet (4B10) and anti-RORγt (Q31–378) was performed following the protocol of Foxp3 Staining buffer set (eBiosciences). Anti-IL-4 (11B11) and anti-IFN-γ (XMG1.2) or corresponding isotype controls were stained after treatment with 2% PFA and 0.15% saponin in PBS-BSA.

Staining of pSTAT5 after IL-15 stimulation was performed following the BD Phosflow protocol. Briefly, thymocytes were incubated in complete RPMI with 100 ng/mL of IL-15 for 20 min (in water bath) together with staining of APC-CD1d/PBS57 tetramer and anti-TCRβ. Cells were fixed with Phosflow™ Fix Buffer I (BD) for 10 min in a 37°C water bath followed by cell permeabilization with prechilled Perm/Wash buffer™ on ice for 30 min pSTAT5 (pY694) was stained after washing with BD Pharmingen™ Stain Buffer. All antibodies were purchased from BD, BioLegend or eBiosciences. Flow cytometry was performed using a FACSCanto II and data were analyzed using FlowJo software.

Antigen presentation assay—Thymocytes isolated from WT and T-*Mettl14*$^{-/-}$ mice were pulsed with α-GalCer ranging from 200 ng/mL to 12.5 ng/mL overnight and irradiated before co-culture with iNKT cell hybridoma (DN32.D3, 5×10^4/well). DN32.D3 cells with knockdown of *Mettl14* (*Mettl14*^{KD}) were stimulated with α-GalCer (200 ng/mL) and supernatants were collected at 24 h for quantification of IL-2 by ELISA as described previously (Weng et al., 2021) or subjected to RNA extraction/qPCR analysis.

Generation of bone marrow chimeras—Bone marrow (BM) cells isolated from WT (CD45.1) and T-*Mettl14*$^{-/-}$ (CD45.2) mice were depleted of mature T cells using anti-Thy-1.2 (AT83.A-6) plus rabbit complement (Cedarlane Laboratories). 1×10^7 BM cells mixed in 1:1 ratio were injected via tail vein into irradiated *Jα18*$^{-/-}$ recipient mice. Six weeks after the BM reconstitution, lymphocytes from recipient mice were isolated from various organs and stained for FACS analysis.

RNA-seq analysis—DP thymocytes from T-*Mettl14*$^{-/-}$ and littermate controls were sorted by BD FACS Aria with purity >98%. RNA was extracted with RNAeasy® mini kit (Qiagen). Libraries were generated by using the Illumina Truseq preparation kit and sequenced on HiSeq4000. Reads were analyzed with Ceto pipeline (https://github.com/ebartom/NGSbartom) using STAR and HTseq for alignment on mm10 mouse genome and reading counting, as described previously (Weng et al., 2021). Paired differential expression analysis was performed using DESeq2 to account for batch differences from two different sorting times (Love et al., 2014). Gene enrichment analysis was performed using GSEA (Subramanian et al., 2005). Data can be accessed at GSE189339.

Real-time PCR—Total RNA from sorted DP thymocytes (CD69$^-$), DN32.D3 and *Vα14*Tg splenocytes was extracted using RNeasy kit (Qiagen) and subjected to cDNA generation using superscript III reverse transcriptase (Invitrogen). Real-time PCR was performed using SYBR green kit (Quantabio) with indicated primers in Key resources table and β-actin was used as control. Primers for *Trim25* and *Xaf1* were purchased from Bio-Rad.

m^{6}A RNA-immunoprecipitation (RNA-IP) and m^{6}A target qPCR analysis—Total RNA was extracted from B6 thymocytes with Trizol (Thermo Fisher), treated with DNase and then incubated with m^{6}A-specific antibody (Sigma) premixed with protein G Dynabeads (Thermo Fisher) and RNasin® Ribonuclease Inhibitors (Promega) overnight on a 360° rotator in 4°C. m^{6}A modified RNA was eluted with 6.7 mM *N*^{6}-methyladenosine 5′-monophosphate sodium salt in IP buffer and re-extracted with Trizol LS (Thermo Fisher).

cDNA was generated from total RNA and m^{6}A modified RNA and subjected to qPCR analysis with indicated primers in Key resources table.

NAC treatment and ROS detection—Thymocytes were incubated with 3 μM CM-H2DCFDA (Thermol Fisher) for 20 min at 37°C and stained for FACS analysis. Thymocytes were incubated for 6 h in complete RPMI medium with or without supplement with 20 mM N-acetyl cysteine (NAC, Sigma) and stained for apoptosis analysis.

Stimulation of DP thymocytes—Sorted DP thymocytes from WT and T-*Mettl14*$^{-/-}$ mice were stimulated with plate-bound anti-CD3 (5 μg/mL) and soluble anti-CD4 (2 μg/mL) for 6 h. Cells were then subjected to Annexin V staining or qPCR analysis. Thymocytes were labeled with CellTrace™ CFSE (Invitrogen) according to the manufacture's protocol and cultured in the presence of IL-2 (200 U/mL) or IL-15 (100 ng/mL). After 3 days, cells were harvested and stained for FACS analysis.

Calcium flux—Thymocytes were labeled with 4 μg/mL Fluro-4 (Invitrogen) and 8 μg/mL Fura-red (Molecular Probes) for 45 min and incubated with biotinylated anti-CD3 (145–2C11) and anti-CD4 (RM4–4) antibodies plus fluorescent-conjugated anti-CD4 (GK1.5) and anti-CD8α (53–6.7). Labeled cells were re-suspended in DPBS without Ca^{2+} and Mg^{2+}, crosslinked by the addition of streptavidin, and then analyzed by flow cytometry. DN32.D3 cells were incubated with 4 μg/mL Fluro-4 and 8 μg/mL Fura-red for 45 min and re-suspended with Ca^{2+}-free DPBS after wash. Ca^{2+}/α-GalCer was introduced for stimulation for flow cytometry analysis.

***In* vivo treatment of α-GalCer—**5 μg of α-GalCer in 200 μL PBS was injected into the tail vein of mice. Lymphocytes were isolated from the liver and spleen in one hour. Cells were cultured for 2 h followed by Monensin treatment for additional 4 h before subjecting to intracellular cytokine staining. Splenic iNKT cells were stained for surface markers, Annexin V and Ki67 on day 3 after *in vivo* α-GalCer injection.

Stable knockdown of *Mettl14* and *Cish* in DN32.D3 NKT cell line—Lentivirus targeting *Mettl14* or negative control (NC) were packaged with a combination of a lentiviral backbone plasmid (pLKO.1, Sigma-Aldrich) and two packaging plasmids, pMD2.G and psPAX2 in 293T cells. pSIREN-RetroQ-Zsgreen plasmid (shLuc as NC) was gifted by Dr. Philip Lazarus (Washington State University) and sh*Cish* was subcloned into *Bam*H I and *Eco*R I sites. Retrovirus were packaged with cotransfection of pSIREN-RetroQ-Zsgreen and pCL-Eco in Phoenix-Eco cells using Lipofectamine LTX reagent according to the manufacture's protocol. The sequences were listed in Key resources table. DN32.D3 cells were transduced by lentivirus encoding *Mettl14*-targeting or NC shRNA (Sigma). Transduced DN32.D3 were selected using complete RPMI 1640 medium supplemented with 5 μg/mL puromycin. Stably transduced cell lines were further spin-transduced with retrovirus expressing shRNA targeting *Cish,* and Zsgreen$^+$ cells were sorted for culture and downstream analysis.

Nucleofection of rCas9/*Mettl14*-gRNA complex in primary iNKT cells—
Splenocytes from $V\alpha14^{Tg}$ mice were isolated with Ficoll-Paque (Sigma) and stimulated as

described previously (Weng et al., 2021). Nucleofection with rCas9 (Thermo Fisher)/gRNA targeting *Mettl14* or scrambled control (Integrated DNA Technologies) was performed using P4 primary cell 4D-NucleofectorTM X Kit S with program CM-137 (Nucleofection Kit; Lonza) (Seki and Rutz, 2018). Splenocytes were further cultured in complete RPMI supplemented with rIL-2 (200 U/mL) for 3 days.

QUANTIFICATION AND STATISTICAL ANALYSIS

Statistics—Statistical analyses were carried out using GraphPad Prism 6.0 (GraphPad Software). Student's t test was used to determine the difference between two groups. A p value < 0.05 was considered statistically significant (*p < 0.05; **p < 0.01; ***p < 0.001). Bar graphs represented mean ± standard error of the mean (SEM). All the statistical details can be found in figure legends.

Supplementary Material

Refer to Web version on PubMed Central for supplementary material.

ACKNOWLEDGMENTS

We thank Dr. Chuan He for the T-*Mettl14*$^{-/-}$ mice, Dr. Albert Bendelac for DN32.D3 NKT cell hybridoma, Dr. Luc Van Kaer for *Jα18*$^{-/-}$ mice, Dr. Elizabeth Bartom for the use of her RNA-seq analysis pipeline, the NIH tetramer core facility for CD1d and MR1 tetramers, Northwestern University flow cytometry core facility for cell sorting, NUSeq core facility for library construction and sequencing, and Northwestern IT Research Computing Services for maintaining the High Performance Computing Cluster Quest. This work was supported by NIH grants R01 AI141083 and R01 AI057460 to C.-R.W.

REFERENCES

Alarcón CR, Lee H, Goodarzi H, Halberg N, and Tavazoie SF (2015). N6-methyladenosine marks primary microRNAs for processing. Nature 519, 482–485. 10.1038/nature14281. [PubMed: 25799998]

Aman MJ, Migone TS, Sasaki A, Ascherman DP, Zhu MH, Soldaini E, Imada K, Miyajima A, Yoshimura A, and Leonard WJ (1999). CIS associates with the interleukin-2 receptor beta chain and inhibits interleukin-2-dependent signaling. J. Biol. Chem 274, 30266–30272. 10.1074/jbc.274.42.30266. [PubMed: 10514520]

Anders S, Pyl PT, and Huber W (2015). HTSeq–a Python framework to work with high-throughput sequencing data. Bioinformatics 31, 166–169. 10.1093/bioinformatics/btu638. [PubMed: 25260700]

Baldwin TA, Hogquist KA, and Jameson SC (2004). The fourth way? Harnessing aggressive tendencies in the thymus. J. Immunol 173, 6515–6520. 10.4049/jimmunol.173.11.6515. [PubMed: 15557139]

Baranek T, Lebrigand K, de Amat Herbozo C, Gonzalez L, Bogard G, Dietrich C, Magnone V, Boisseau C, Jouan Y, Trottein F, et al. (2020). High dimensional single-cell analysis reveals iNKT cell developmental trajectories and effector fate decision. Cell Rep 32, 108116. 10.1016/j.celrep.2020.108116. [PubMed: 32905761]

Batista PJ, Molinie B, Wang J, Qu K, Zhang J, Li L, Bouley DM, Lujan E, Haddad B, Daneshvar K, et al. (2014). m(6)A RNA modification controls cell fate transition in mammalian embryonic stem cells. Cell Stem Cell 15, 707–719. 10.1016/j.stem.2014.09.019. [PubMed: 25456834]

Bedard M, Salio M, and Cerundolo V (2017). Harnessing the power of invariant natural killer T cells in cancer immunotherapy. Front. Immunol 8, 1829. 10.3389/fimmu.2017.01829. [PubMed: 29326711]

Bendelac A (1995). Positive selection of mouse NK1+ T cells by CD1-expressing cortical thymocytes. J. Exp. Med 182, 2091–2096. 10.1084/jem.182.6.2091. [PubMed: 7500054]

Bendelac A, Savage PB, and Teyton L (2007). The biology of NKT cells. Annu. Rev. Immunol 25, 297–336. 10.1146/annurev.immunol.25.022106.141711. [PubMed: 17150027]

Benlagha K, Wei DG, Veiga J, Teyton L, and Bendelac A (2005). Characterization of the early stages of thymic NKT cell development. J. Exp. Med 202, 485–492. 10.1084/jem.20050456. [PubMed: 16087715]

Bolger AM, Lohse M, and Usadel B (2014). Trimmomatic: a flexible trimmer for Illumina sequence data. Bioinformatics 30, 2114–2120. 10.1093/bioinformatics/btu170. [PubMed: 24695404]

Brocker CN, Kim D, Melia T, Karri K, Velenosi TJ, Takahashi S, Aibara D, Bonzo JA, Levi M, Waxman DJ, and Gonzalez FJ (2020). Long non-coding RNA Gm15441 attenuates hepatic inflammasome activation in response to PPARA agonism and fasting. Nat. Commun 11, 5847. 10.1038/s41467-020-19554-7. [PubMed: 33203882]

Cheng C, Wu Y, Xiao T, Xue J, Sun J, Xia H, Ma H, Lu L, Li J, Shi A, et al. (2021). METTL3-mediated m(6)A modification of ZBTB4 mRNA is involved in the smoking-induced EMT in cancer of the lung. Mol. Ther. Nucleic Acids 23, 487–500. 10.1016/j.omtn.2020.12.001. [PubMed: 33510938]

Choe J, Lin S, Zhang W, Liu Q, Wang L, Ramirez-Moya J, Du P, Kim W, Tang S, Sliz P, et al. (2018). mRNA circularization by METTL3-eIF3h enhances translation and promotes oncogenesis. Nature 561, 556–560. 10.1038/s41586-018-0538-8. [PubMed: 30232453]

Constantinides MG, and Bendelac A (2013). Transcriptional regulation of the NKT cell lineage. Curr. Opin. Immunol 25, 161–167. 10.1016/j.coi.2013.01.003. [PubMed: 23402834]

Crosby CM, and Kronenberg M (2018). Tissue-specific functions of invariant natural killer T cells. Nat. Rev. Immunol 18, 559–574. 10.1038/s41577-018-0034-2. [PubMed: 29967365]

Cui J, Shin T, Kawano T, Sato H, Kondo E, Toura I, Kaneko Y, Koseki H, Kanno M, and Taniguchi M (1997). Requirement for Valpha14 NKT cells in IL-12-mediated rejection of tumors. Science 278, 1623–1626. 10.1126/science.278.5343.1623. [PubMed: 9374462]

Dobin A, Davis CA, Schlesinger F, Drenkow J, Zaleski C, Jha S, Batut P, Chaisson M, and Gingeras TR (2013). STAR: ultrafast universal RNA-seq aligner. Bioinformatics 29, 15–21. 10.1093/bioinformatics/bts635. [PubMed: 23104886]

Dolbois A, Bedi RK, Bochenkova E, Müller A, Moroz-Omori EV, Huang D, and Caflisch A (2021). 1, 4, 9-Triazaspiro[5.5]undecan-2-one derivatives as potent and selective METTL3 inhibitors. J. Med. Chem 64, 12738–12760. 10.1021/acs.jmedchem.1c00773. [PubMed: 34431664]

Dominissini D, Moshitch-Moshkovitz S, Schwartz S, Salmon-Divon M, Ungar L, Osenberg S, Cesarkas K, Jacob-Hirsch J, Amariglio N, Kupiec M, et al. (2012). Topology of the human and mouse m6A RNA methylomes revealed by m6A-seq. Nature 485, 201–206. 10.1038/nature11112. [PubMed: 22575960]

Dose M, Sleckman BP, Han J, Bredemeyer AL, Bendelac A, and Gounari F (2009). Intrathymic proliferation wave essential for Valpha14+ natural killer T cell development depends on c-Myc. Proc. Natl. Acad. Sci. USA 106, 8641–8646. 10.1073/pnas.0812255106. [PubMed: 19423665]

Engel I, Seumois G, Chavez L, Samaniego-Castruita D, White B, Chawla A, Mock D, Vijayanand P, and Kronenberg M (2016). Innate-like functions of natural killer T cell subsets result from highly divergent gene programs. Nat. Immunol 17, 728–739. 10.1038/ni.3437. [PubMed: 27089380]

Erson-Bensan AE, and Begik O (2017). m6A Modification and Implications for microRNAs. MicroRNA 6, 97–101. 10.2174/2211536606666170511102219. [PubMed: 28494721]

Fernandes JCR, Acuña SM, Aoki JI, Floeter-Winter LM, and Muxel SM (2019). Long non-coding RNAs in the regulation of gene expression: physiology and disease. Noncoding RNA 5, 17. 10.3390/ncrna5010017.

Frasca F, Rustighi A, Malaguarnera R, Altamura S, Vigneri P, Del Sal G, Giancotti V, Pezzino V, Vigneri R, and Manfioletti G (2006). HMGA1 inhibits the function of p53 family members in thyroid cancer cells. Cancer Res 66, 2980–2989. 10.1158/0008-5472.CAN-05-2637. [PubMed: 16540646]

Fujii SI, and Shimizu K (2019). Immune networks and therapeutic targeting of iNKT cells in cancer. Trends Immunol 40, 984–997. 10.1016/j.it.2019.09.008. [PubMed: 31676264]

Funakoshi-Tago M, Moriwaki T, Ueda F, Tamura H, Kasahara T, and Tago K (2017). Phosphorylated CIS suppresses the Epo or JAK2 V617F mutant-triggered cell proliferation through binding to EpoR. Cell. Signal 31, 41–57. 10.1016/j.cellsig.2016.12.008. [PubMed: 28038963]

Gálvez NMS, Bohmwald K, Pacheco GA, Andrade CA, Carreño LJ, and Kalergis AM (2021). Type I natural killer T cells as key regulators of the immune response to infectious diseases. Clin. Microbiol. Rev 34, e00232–20. 10.1128/CMR.00232-20. [PubMed: 33361143]

Geula S, Moshitch-Moshkovitz S, Dominissini D, Mansour AA, Kol N, Salmon-Divon M, Hershkovitz V, Peer E, Mor N, Manor YS, et al. (2015). Stem cells. m6A mRNA methylation facilitates resolution of naive pluripotency toward differentiation. Science 347, 1002–1006. 10.1126/science.1261417. [PubMed: 25569111]

Godfrey DI, Stankovic S, and Baxter AG (2010). Raising the NKT cell family. Nat. Immunol 11, 197–206. 10.1038/ni.1841. [PubMed: 20139988]

Goossens PL, Jouin H, Marchal G, and Milon G (1990). Isolation and flow cytometric analysis of the free lymphomyeloid cells present in murine liver. J. Immunol. Methods 132, 137–144. 10.1016/0022-1759(90)90407-m. [PubMed: 2202764]

Gordy LE, Bezbradica JS, Flyak AI, Spencer CT, Dunkle A, Sun J, Stanic AK, Boothby MR, He YW, Zhao Z, et al. (2011). IL-15 regulates homeostasis and terminal maturation of NKT cells. J. Immunol 187, 6335–6345. 10.4049/jimmunol.1003965. [PubMed: 22084435]

Griewank K, Borowski C, Rietdijk S, Wang N, Julien A, Wei DG, Mamchak AA, Terhorst C, and Bendelac A (2007). Homotypic interactions mediated by Slamf1 and Slamf6 receptors control NKT cell lineage development. Immunity 27, 751–762. 10.1016/j.immuni.2007.08.020. [PubMed: 18031695]

Harsha Krovi S, Zhang J, Michaels-Foster MJ, Brunetti T, Loh L, Scott-Browne J, and Gapin L (2020). Thymic iNKT single cell analyses unmask the common developmental program of mouse innate T cells. Nat. Commun 11, 6238. 10.1038/s41467-020-20073-8. [PubMed: 33288744]

He PC, and He C (2021). m(6) A RNA methylation: from mechanisms to therapeutic potential. EMBO J 40, e105977. 10.15252/embj.2020105977. [PubMed: 33470439]

He RZ, Jiang J, and Luo DX (2020). The functions of N6-methyladenosine modification in lncRNAs. Genes Dis 7, 598–605. 10.1016/j.gendis.2020.03.005. [PubMed: 33335959]

Heller JJ, Schjerven H, Li S, Lee A, Qiu J, Chen ZME, Smale ST, and Zhou L (2014). Restriction of IL-22-producing T cell responses and differential regulation of regulatory T cell compartments by zinc finger transcription factor Ikaros. J. Immunol 193, 3934–3946. 10.4049/jimmunol.1401234. [PubMed: 25194055]

Hu T, Simmons A, Yuan J, Bender TP, and Alberola-Ila J (2010). The transcription factor c-Myb primes CD4+CD8+ immature thymocytes for selection into the iNKT lineage. Nat. Immunol 11, 435–441. 10.1038/ni.1865. [PubMed: 20383148]

Johnson TM, Yu ZX, Ferrans VJ, Lowenstein RA, and Finkel T (1996). Reactive oxygen species are downstream mediators of p53-dependent apoptosis. Proc. Natl. Acad. Sci. USA 93, 11848–11852. 10.1073/pnas.93.21.11848. [PubMed: 8876226]

Juno JA, Keynan Y, and Fowke KR (2012). Invariant NKT cells: regulation and function during viral infection. PLoS Pathog 8, e1002838. 10.1371/journal.ppat.1002838. [PubMed: 22916008]

Kim YH, Kumar A, Chang CH, and Pyaram K (2017). Reactive oxygen species regulate the inflammatory function of NKT cells through promyelocytic leukemia zinc finger. J. Immunol 199, 3478–3487. 10.4049/jimmunol.1700567. [PubMed: 29021374]

Kishimoto H, Ohteki T, Yajima N, Kawahara K, Natsui M, Kawarasaki S, Hamada K, Horie Y, Kubo Y, Arase S, et al. (2007). The Pten/PI3K pathway governs the homeostasis of Valpha14iNKT cells. Blood 109, 3316–3324. 10.1182/blood-2006-07-038059. [PubMed: 17170126]

Kobayashi M, Ohsugi M, Sasako T, Awazawa M, Umehara T, Iwane A, Kobayashi N, Okazaki Y, Kubota N, Suzuki R, et al. (2018). The RNA meth-yltransferase complex of WTAP, METTL3, and METTL14 regulates mitotic clonal expansion in adipogenesis. Mol. Cell Biol 38, e00116–18. 10.1128/MCB.00116-18. [PubMed: 29866655]

Koseki H, Asano H, Inaba T, Miyashita N, Moriwaki K, Lindahl KF, Mizutani Y, Imai K, and Taniguchi M (1991). Dominant expression of a distinctive V14+ T-cell antigen receptor alpha chain in mice. Proc. Natl. Acad. Sci. USA 88, 7518–7522. 10.1073/pnas.88.17.7518. [PubMed: 1881891]

Kovalovsky D, Uche OU, Eladad S, Hobbs RM, Yi W, Alonzo E, Chua K, Eidson M, Kim HJ, Im JS, et al. (2008). The BTB-zinc finger transcriptional regulator PLZF controls the development of invariant natural killer T cell effector functions. Nat. Immunol 9, 1055–1064. 10.1038/ni.1641. [PubMed: 18660811]

Kronenberg M (2005). Toward an understanding of NKT cell biology: progress and paradoxes. Annu. Rev. Immunol 23, 877–900. 10.1146/annurev.immunol.23.021704.115742. [PubMed: 15771592]

Lan Q, Liu PY, Haase J, Bell JL, Hüttelmaier S, and Liu T (2019). The critical role of RNA m(6)A methylation in cancer. Cancer Res 79, 1285–1292. 10.1158/0008-5472.CAN-18-2965. [PubMed: 30894375]

Lantz O, and Bendelac A (1994). An invariant T cell receptor alpha chain is used by a unique subset of major histocompatibility complex class I-specific CD4+ and CD4–8- T cells in mice and humans. J. Exp. Med 180, 1097–1106. 10.1084/jem.180.3.1097. [PubMed: 7520467]

Lazarevic V, Zullo AJ, Schweitzer MN, Staton TL, Gallo EM, Crabtree GR, and Glimcher LH (2009). The gene encoding early growth response 2, a target of the transcription factor NFAT, is required for the development and maturation of natural killer T cells. Nat. Immunol 10, 306–313. 10.1038/ni.1696. [PubMed: 19169262]

Lee M, Lee E, Han SK, Choi YH, Kwon DI, Choi H, Lee K, Park ES, Rha MS, Joo DJ, et al. (2020). Single-cell RNA sequencing identifies shared differentiation paths of mouse thymic innate T cells. Nat. Commun 11, 4367. 10.1038/s41467-020-18155-8. [PubMed: 32868763]

Lee MG, Han J, Jeong SI, Her NG, Lee JH, Ha TK, Kang MJ, Ryu BK, and Chi SG (2014). XAF1 directs apoptotic switch of p53 signaling through activation of HIPK2 and ZNF313. Proc. Natl. Acad. Sci. USA 111, 15532–15537. 10.1073/pnas.1411746111. [PubMed: 25313037]

Lee YJ, Holzapfel KL, Zhu J, Jameson SC, and Hogquist KA (2013). Steady-state production of IL-4 modulates immunity in mouse strains and is determined by lineage diversity of iNKT cells. Nat. Immunol 14, 1146–1154. 10.1038/ni.2731. [PubMed: 24097110]

Li HB, Tong J, Zhu S, Batista PJ, Duffy EE, Zhao J, Bailis W, Cao G, Kroehling L, Chen Y, et al. (2017). m(6)A mRNA methylation controls T cell homeostasis by targeting the IL-7/STAT5/SOCS pathways. Nature 548, 338–342. 10.1038/nature23450. [PubMed: 28792938]

Li S, Chen S, Xu X, Sundstedt A, Paulsson KM, Anderson P, Karlsson S, Sjögren HO, and Wang P (2000). Cytokine-induced Src homology 2 protein (CIS) promotes T cell receptor-mediated proliferation and prolongs survival of activated T cells. J. Exp. Med 191, 985–994. 10.1084/jem.191.6.985. [PubMed: 10727460]

Lin S, Choe J, Du P, Triboulet R, and Gregory RI (2016). The m(6)A methyltransferase METTL3 promotes translation in human cancer cells. Mol. Cell 62, 335–345. 10.1016/j.molcel.2016.03.021. [PubMed: 27117702]

Liu J, Yue Y, Han D, Wang X, Fu Y, Zhang L, Jia G, Yu M, Lu Z, Deng X, et al. (2014). A METTL3-METTL14 complex mediates mammalian nuclear RNA N6-adenosine methylation. Nat. Chem. Biol 10, 93–95. 10.1038/nchembio.1432. [PubMed: 24316715]

Liu Y, Tao S, Liao L, Li Y, Li H, Li Z, Lin L, Wan X, Yang X, and Chen L (2020). TRIM25 promotes the cell survival and growth of hepatocellular carcinoma through targeting Keap1-Nrf2 pathway. Nat. Commun 11, 348. 10.1038/s41467-019-14190-2. [PubMed: 31953436]

Love MI, Huber W, and Anders S (2014). Moderated estimation of fold change and dispersion for RNA-seq data with DESeq2. Genome Biol 15, 550. 10.1186/s13059-014-0550-8. [PubMed: 25516281]

Lu TX, Zheng Z, Zhang L, Sun HL, Bissonnette M, Huang H, and He C (2020). A new model of spontaneous colitis in mice induced by deletion of an RNA m(6)A methyltransferase component METTL14 in T cells. Cell Mol. Gastroenterol. Hepatol 10, 747–761. 10.1016/j.jcmgh.2020.07.001.

Mandal M, Chen XR, Alegre ML, Chiu NM, Chen YH, Castaño AR, and Wang CR (1998). Tissue distribution, regulation and intracellular localization of murine CD1 molecules. Mol. Immunol 35, 525–536. 10.1016/s0161-5890(98)00055-8. [PubMed: 9809580]

Manners O, Baquero-Perez B, and Whitehouse A (2019). m(6)A: wide-spread regulatory control in virus replication. Biochim. Biophys. Acta. Gene Regul. Mech 1862, 370–381. 10.1016/j.bbagrm.2018.10.015. [PubMed: 30412798]

Mathur L, Jung S, Jang C, and Lee G (2021). Quantitative analysis of m(6) A RNA modification by LC-MS. STAR Protoc 2, 100724. 10.1016/j.xpro.2021.100724. [PubMed: 34401789]

Matsuda JL, Gapin L, Sidobre S, Kieper WC, Tan JT, Ceredig R, Surh CD, and Kronenberg M (2002). Homeostasis of V alpha 14i NKT cells. Nat. Immunol 3, 966–974. 10.1038/ni837. [PubMed: 12244311]

Matsumoto A, Masuhara M, Mitsui K, Yokouchi M, Ohtsubo M, Misawa H, Miyajima A, and Yoshimura A (1997). CIS, a cytokine inducible SH2 protein, is a target of the JAK-STAT5 pathway and modulates STAT5 activation. Blood 89, 3148–3154. [PubMed: 9129017]

Meyer KD, and Jaffrey SR (2014). The dynamic epitranscriptome: N6-methyladenosine and gene expression control. Nat. Rev. Mol. Cell Biol 15, 313–326. 10.1038/nrm3785. [PubMed: 24713629]

Moran AE, Holzapfel KL, Xing Y, Cunningham NR, Maltzman JS, Punt J, and Hogquist KA (2011). T cell receptor signal strength in Treg and iNKT cell development demonstrated by a novel fluorescent reporter mouse. J. Exp. Med 208, 1279–1289. 10.1084/jem.20110308. [PubMed: 21606508]

Moroz-Omori EV, Huang D, Kumar Bedi R, Cheriyamkunnel SJ, Bochenkova E, Dolbois A, Rzeczkowski MD, Li Y, Wiedmer L, and Caflisch A (2021). METTL3 inhibitors for epitranscriptomic modulation of cellular processes. ChemMedChem 16, 3035–3043. 10.1002/cmdc.202100291. [PubMed: 34237194]

Mycko MP, Ferrero I, Wilson A, Jiang W, Bianchi T, Trumpp A, and MacDonald HR (2009). Selective requirement for c-Myc at an early stage of V(alpha)14i NKT cell development. J. Immunol 182, 4641–4648. 10.4049/jimmunol.0803394. [PubMed: 19342639]

Oh SJ, Ahn S, Jin YH, Ishifune C, Kim JH, Yasutomo K, and Chung DH (2015). Notch 1 and Notch 2 synergistically regulate the differentiation and function of invariant NKT cells. J. Leukoc. Biol 98, 781–789. 10.1189/jlb.1A0914-459RR. [PubMed: 26188077]

Palmer DC, Guittard GC, Franco Z, Crompton JG, Eil RL, Patel SJ, Ji Y, Van Panhuys N, Klebanoff CA, Sukumar M, et al. (2015). Cish actively silences TCR signaling in CD8+ T cells to maintain tumor tolerance. J. Exp. Med 212, 2095–2113. 10.1084/jem.20150304. [PubMed: 26527801]

Pathak N, and Khandelwal S (2006). Influence of cadmium on murine thymocytes: potentiation of apoptosis and oxidative stress. Toxicol. Lett 165, 121–132. 10.1016/j.toxlet.2006.02.004. [PubMed: 16563667]

Pellicci DG, Hammond KJL, Uldrich AP, Baxter AG, Smyth MJ, and Godfrey DI (2002). A natural killer T (NKT) cell developmental pathway iInvolving a thymus-dependent NK1.1(-)CD4(+) CD1d-dependent precursor stage. J. Exp. Med 195, 835–844. 10.1084/jem.20011544. [PubMed: 11927628]

Ping XL, Sun BF, Wang L, Xiao W, Yang X, Wang WJ, Adhikari S, Shi Y, Lv Y, Chen YS, et al. (2014). Mammalian WTAP is a regulatory subunit of the RNA N6-methyladenosine methyltransferase. Cell Res 24, 177–189. 10.1038/cr.2014.3. [PubMed: 24407421]

Prima V, Kaliberova LN, Kaliberov S, Curiel DT, and Kusmartsev S (2017). COX2/mPGES1/PGE2 pathway regulates PD-L1 expression in tumor-associated macrophages and myeloid-derived suppressor cells. Proc. Natl. Acad. Sci. USA 114, 1117–1122. 10.1073/pnas.1612920114. [PubMed: 28096371]

Pyaram K, Kumar A, Kim YH, Noel S, Reddy SP, Rabb H, and Chang CH (2019). Keap1-Nrf2 system plays an important role in invariant natural killer T cell development and homeostasis. Cell Rep 27, 699–707.e4. 10.1016/j.celrep.2019.03.052. [PubMed: 30995469]

Roignant JY, and Soller M (2017). m(6)A in mRNA: an ancient mechanism for fine-tuning gene expression. Trends Genet 33, 380–390. 10.1016/j.tig.2017.04.003. [PubMed: 28499622]

Rossjohn J, Pellicci DG, Patel O, Gapin L, and Godfrey DI (2012). Recognition of CD1d-restricted antigens by natural killer T cells. Nat. Rev. Immunol 12, 845–857. 10.1038/nri3328. [PubMed: 23154222]

Roundtree IA, Evans ME, Pan T, and He C (2017). Dynamic RNA modifications in gene expression regulation. Cell 169, 1187–1200. 10.1016/j.cell.2017.05.045. [PubMed: 28622506]

Savage AK, Constantinides MG, Han J, Picard D, Martin E, Li B, Lantz O, and Bendelac A (2008). The transcription factor PLZF directs the effector program of the NKT cell lineage. Immunity 29, 391–403. 10.1016/j.immuni.2008.07.011. [PubMed: 18703361]

Seiler MP, Mathew R, Liszewski MK, Spooner CJ, Spooner C, Barr K, Meng F, Singh H, and Bendelac A (2012). Elevated and sustained expression of the transcription factors Egr1 and Egr2 controls NKT lineage differentiation in response to TCR signaling. Nat. Immunol 13, 264–271. 10.1038/ni.2230. [PubMed: 22306690]

Seki A, and Rutz S (2018). Optimized RNP transfection for highly efficient CRISPR/Cas9-mediated gene knockout in primary T cells. J. Exp. Med 215, 985–997. 10.1084/jem.20171626. [PubMed: 29436394]

Sena LA, Li S, Jairaman A, Prakriya M, Ezponda T, Hildeman DA, Wang CR, Schumacker PT, Licht JD, Perlman H, et al. (2013). Mitochondria are required for antigen-specific T cell activation through reactive oxygen species signaling. Immunity 38, 225–236. 10.1016/j.immuni.2012.10.020. [PubMed: 23415911]

Shafik A, Schumann U, Evers M, Sibbritt T, and Preiss T (2016). The emerging epitranscriptomics of long noncoding RNAs. Biochim. Biophys. Acta 1859, 59–70. 10.1016/j.bbagrm.2015.10.019. [PubMed: 26541084]

Sintes J, Cuenca M, Romero X, Bastos R, Terhorst C, Angulo A, and Engel P (2013). Cutting edge: Ly9 (CD229), a SLAM family receptor, negatively regulates the development of thymic innate memory-like CD8+ T and invariant NKT cells. J. Immunol 190, 21–26. 10.4049/jimmunol.1202435. [PubMed: 23225888]

Slauenwhite D, and Johnston B (2015). Regulation of NKT cell localization in homeostasis and infection. Front. Immunol 6, 255. 10.3389/fimmu.2015.00255. [PubMed: 26074921]

Song H, Song J, Cheng M, Zheng M, Wang T, Tian S, Flavell RA, Zhu S, Li HB, Ding C, et al. (2021). METTL3-mediated m(6)A RNA methylation promotes the anti-tumour immunity of natural killer cells. Nat. Commun 12, 5522. 10.1038/s41467-021-25803-0. [PubMed: 34535671]

Stanic AK, Bezbradica JS, Park JJ, Van Kaer L, Boothby MR, and Joyce S (2004). Cutting edge: the ontogeny and function of Va14Ja18 natural T lymphocytes require signal processing by protein kinase C theta and NF-kappa B. J. Immunol 172, 4667–4671. 10.4049/jimmunol.172.8.4667. [PubMed: 15067039]

Subramanian A, Tamayo P, Mootha VK, Mukherjee S, Ebert BL, Gillette MA, Paulovich A, Pomeroy SL, Golub TR, Lander ES, and Mesirov JP (2005). Gene set enrichment analysis: a knowledge-based approach for interpreting genome-wide expression profiles. Proc. Natl. Acad. Sci. USA 102, 15545–15550. 10.1073/pnas.0506580102. [PubMed: 16199517]

Terabe M, and Berzofsky JA (2018). Tissue-specific roles of NKT cells in tumor immunity. Front. Immunol 9, 1838. 10.3389/fimmu.2018.01838. [PubMed: 30158927]

Tong J, Cao G, Zhang T, Sefik E, Amezcua Vesely MC, Broughton JP, Zhu S, Li H, Li B, Chen L, et al. (2018). m(6)A mRNA methylation sustains Treg suppressive functions. Cell Res 28, 253–256. 10.1038/cr.2018.7. [PubMed: 29303144]

Van Kaer L, and Wu L (2018). Therapeutic potential of invariant natural killer T cells in autoimmunity. Front. Immunol 9, 519. 10.3389/fimmu.2018.00519. [PubMed: 29593743]

Wang H, and Hogquist KA (2018). CCR7 defines a precursor for murine iNKT cells in thymus and periphery. Elife 7, e34793. 10.7554/eLife.34793. [PubMed: 30102153]

Wang H, Hu X, Huang M, Liu J, Gu Y, Ma L, Zhou Q, and Cao X (2019). Mettl3-mediated mRNA m(6)A methylation promotes dendritic cell activation. Nat. Commun 10, 1898. 10.1038/s41467-019-09903-6. [PubMed: 31015515]

Weng X, Kumar A, Cao L, He Y, Morgun E, Visvabharathy L, Zhao J, Sena LA, Weinberg SE, Chandel NS, and Wang CR (2021). Mitochondrial metabolism is essential for invariant natural killer T cell development and function. Proc. Natl. Acad. Sci. USA 118, e2021385118. 10.1073/pnas.2021385118. [PubMed: 33753493]

Yankova E, Blackaby W, Albertella M, Rak J, De Braekeleer E, Tsagkogeorga G, Pilka ES, Aspris D, Leggate D, Hendrick AG, et al. (2021). Small-molecule inhibition of METTL3 as a strategy against myeloid leukaemia. Nature 593, 597–601. 10.1038/s41586-021-03536-w. [PubMed: 33902106]

Yao Y, Yang Y, Guo W, Xu L, You M, Zhang YC, Sun Z, Cui X, Yu G, Qi Z, et al. (2021). METTL3-dependent m(6)A modification programs T follicular helper cell differentiation. Nat. Commun 12, 1333. 10.1038/s41467-021-21594-6. [PubMed: 33637761]

Yoshimura A, Ohkubo T, Kiguchi T, Jenkins NA, Gilbert DJ, Copeland NG, Hara T, and Miyajima A (1995). A novel cytokine-inducible gene CIS encodes an SH2-containing protein that binds to tyrosine-phosphorylated interleukin 3 and erythropoietin receptors. EMBO J 14, 2816–2826. [PubMed: 7796808]

You XY, Huang JH, Liu B, Liu SJ, Zhong Y, and Liu SM (2014). HMGA1 is a new target of miR-195 involving isoprenaline-induced cardiomyocyte hypertrophy. Biochemistry 79, 538–544. 10.1134/S0006297914060078. [PubMed: 25100012]

Zhao J, Weng X, Bagchi S, and Wang CR (2014). Polyclonal type II natural killer T cells require PLZF and SAP for their development and contribute to CpG-mediated antitumor response. Proc. Natl. Acad. Sci. USA 111, 2674–2679. 10.1073/pnas.1323845111. [PubMed: 24550295]

Zhao T, Sun D, Zhao M, Lai Y, Liu Y, and Zhang Z (2020). N(6)-methyladenosine mediates arsenite-induced human keratinocyte transformation by suppressing p53 activation. Environ. Pollut 259, 113908. 10.1016/j.envpol.2019.113908. [PubMed: 31931413]

Zheng Z, Zhang L, Cui XL, Yu X, Hsu PJ, Lyu R, Tan H, Mandal M, Zhang M, Sun HL, et al. (2020). Control of early B cell development by the RNA N(6)-methyladenosine methylation. Cell Rep 31, 107819. 10.1016/j.celrep.2020.107819. [PubMed: 32610122]

Zhu L, Xie X, Zhang L, Wang H, Jie Z, Zhou X, Shi J, Zhao S, Zhang B, Cheng X, and Sun SC (2018). TBK-binding protein 1 regulates IL-15-induced autophagy and NKT cell survival. Nat. Commun 9, 2812. 10.1038/s41467-018-05097-5. [PubMed: 30022064]

Zimmer MI, Colmone A, Felio K, Xu H, Ma A, and Wang CR (2006). A cell-type specific CD1d expression program modulates invariant NKT cell development and function. J. Immunol 176, 1421–1430. 10.4049/jimmunol.176.3.1421. [PubMed: 16424169]

Highlights

- RNA m^6A methylation plays essential roles in iNKT cell development and function
- Reduced m^6A RNA methylation enhances iNKT cell apoptosis in thymus and periphery
- Loss of METTL14 diminishes TCR signaling and cytokine response in iNKT cells

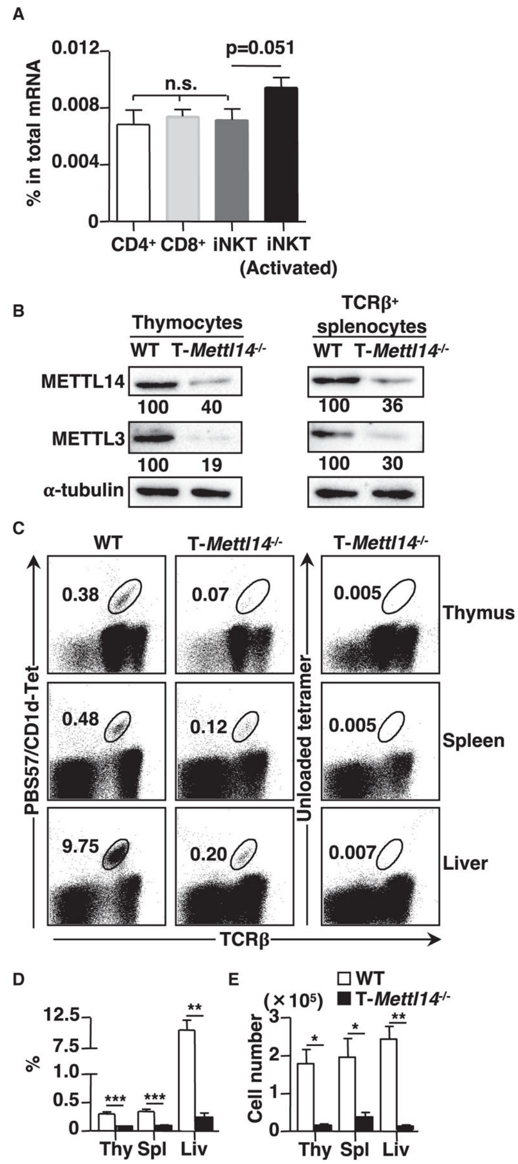

Figure 1. iNKT cell development is severely impaired in T-*Mettl14*$^{-/-}$ mice

(A) m^{6}A level in total mRNA of CD4$^+$, CD8$^+$ T cells, and iNKT cells (naive and activated) (n = 5–6).

(B) Immunoblot of METTL14 and METTL3 in total thymocytes and TCRβ$^+$ splenocytes in WT and T-*Mettl14*$^{-/-}$ mice. Data representative of three independent experiments.

(C) Representative staining of lymphocytes in indicated organs from WT and T-*Mettl14*$^{-/-}$ mice with CD1d/PBS57 tetramer or unloaded CD1d tetramer.

(D and E) Summary of frequencies and cell numbers of iNKT cells in the indicated organs from WT and T-*Mettl14*$^{-/-}$ mice (n = 5–8). SEM is shown. *$p < 0.05$, **$p < 0.01$, ***$p < 0.001$.

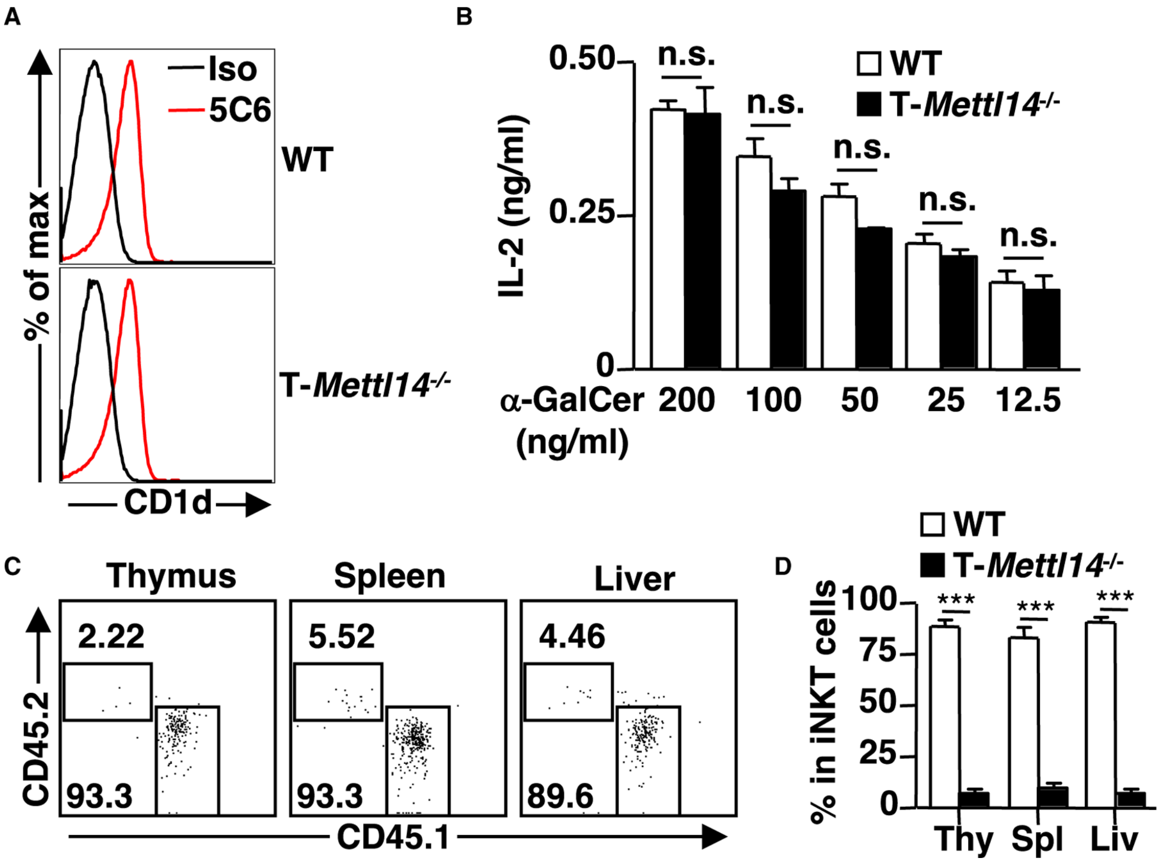

Figure 2. Defective development of iNKT cells in T-*Mettl14*$^{-/-}$ mice is cell intrinsic

(A) Representative histogram of CD1d expression on DP thymocytes. CD1d was stained with α-CD1d or isotype control antibody (n = 8).

(B) IL-2 detected by ELISA following 48-h co-culture of iNKT cell hybridoma DN32.D3 with irradiated thymocytes pulsed with α-GalCer ranging from 200 ng/mL to 12.5 ng/mL. Data representative of three independent experiments.

(C) Flow cytometric analysis of iNKT cells in the *Jα18*$^{-/-}$ recipient mice after 6 weeks of reconstitution with 1:1 mixture of bone marrow cells from WT (CD45.1) and T-*Mettl14*$^{-/-}$ (CD45.2).

(D) Quantification of iNKT cell reconstitution in thymus, spleen, and liver in bone marrow chimera recipients (n = 7). SEM is shown. ***p < 0.001.

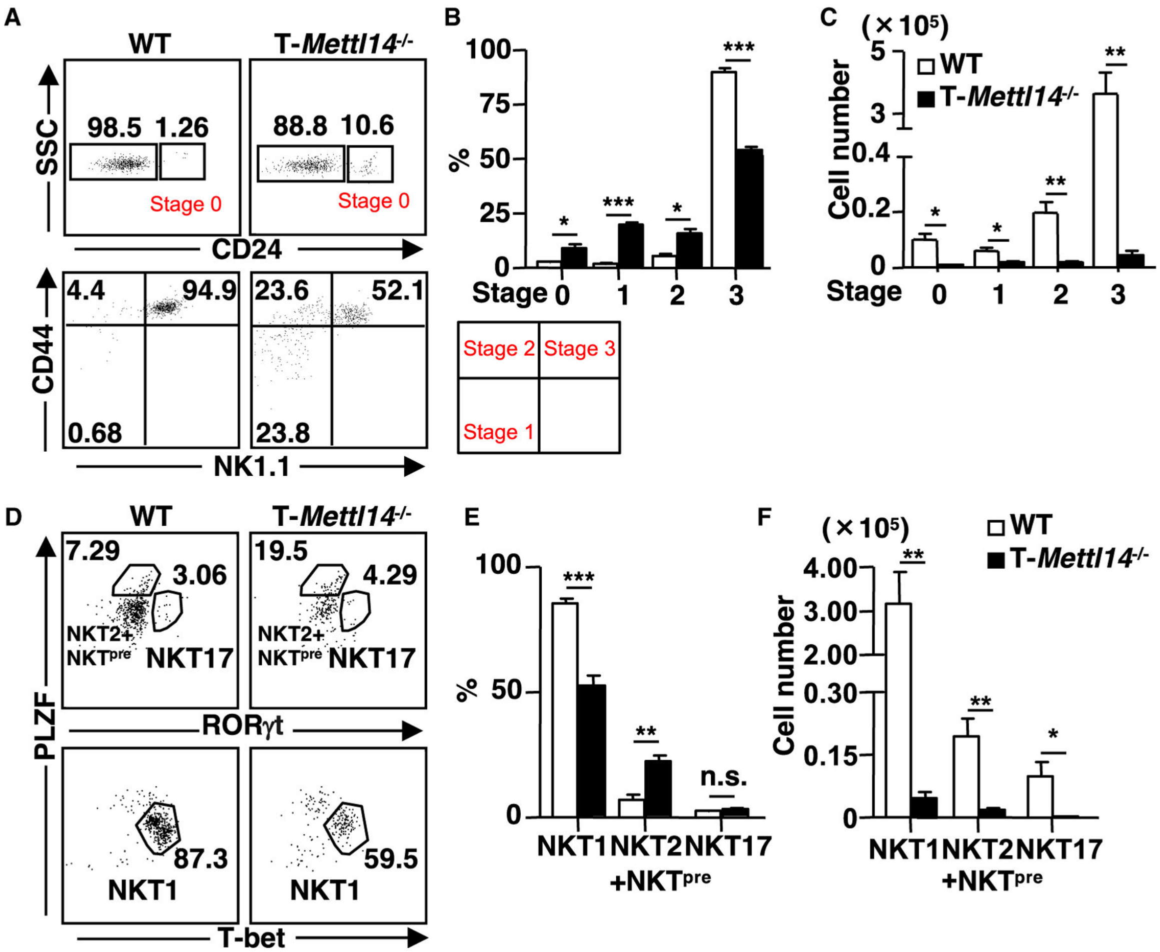

Figure 3. ***Mettl14*** **deficiency impairs the maturation of iNKT cells**

(A) Representative staining of iNKT cells (CD69$^+$CD1d/PBS57 tetramer$^+$) at various developmental stages in the thymus of WT and T-*Mettl14*$^{-/-}$ mice.

(B and C) Quantification of percentages and cell numbers of stages 0, 1, 2, and 3 iNKT cells in WT and T-*Mettl14*$^{-/-}$ mice (n = 3–4).

(D) Intracellular staining of PLZF, T-bet, and RORγt in thymic iNKT cells of WT and T-*Mettl14*$^{-/-}$ mice.

(E and F) Quantification of percentages and cell numbers of NKT1, NKT2+NKT^{pre}, and NKT17 subsets (n = 6). SEM is shown. *p < 0.05, **p < 0.01, ***p < 0.001.

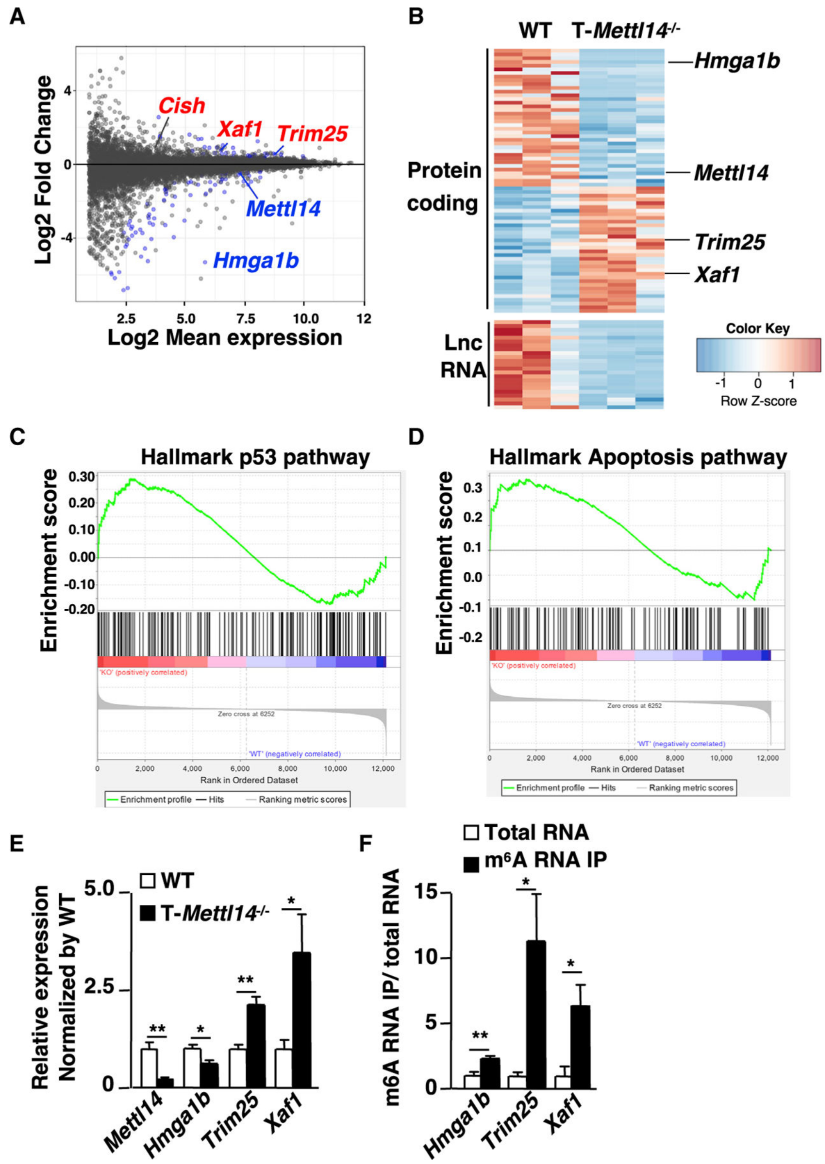

Figure 4. m^{6}A maintains DP thymocyte survival in part through regulation of the p53-mediated apoptosis pathway

(A) RNA-seq results of DP thymocytes from WT and T-*Mettl14*$^{-/-}$ mice with indicated gene labeling (n = 3). Data shown are fold change of T-*Mettl14*$^{-/-}$/WT.

(B) Heatmap of differentially expressed protein-coding genes and long non-coding RNA. Gene set enrichment analysis showing enrichment for hallmark p53 pathway (C) and apoptosis pathway (D) in T-*Mettl14*$^{-/-}$ DP thymocytes.

(E) Relative expression of *Mettl14*, *Hmga1b*, *Trim25*, and *Xaf1* in DP thymocytes of T-*Mettl14*$^{-/-}$ mice detected by qPCR.

(F) Relative expression of *Hmga1b*, *Trim25*, and *Xaf1* in the m^{6}A RNA immunoprecipitation versus total thymocyte RNA in WT mice detected by qPCR (n = 3–4). SEM is shown. *$p < 0.05$, **$p < 0.01$.

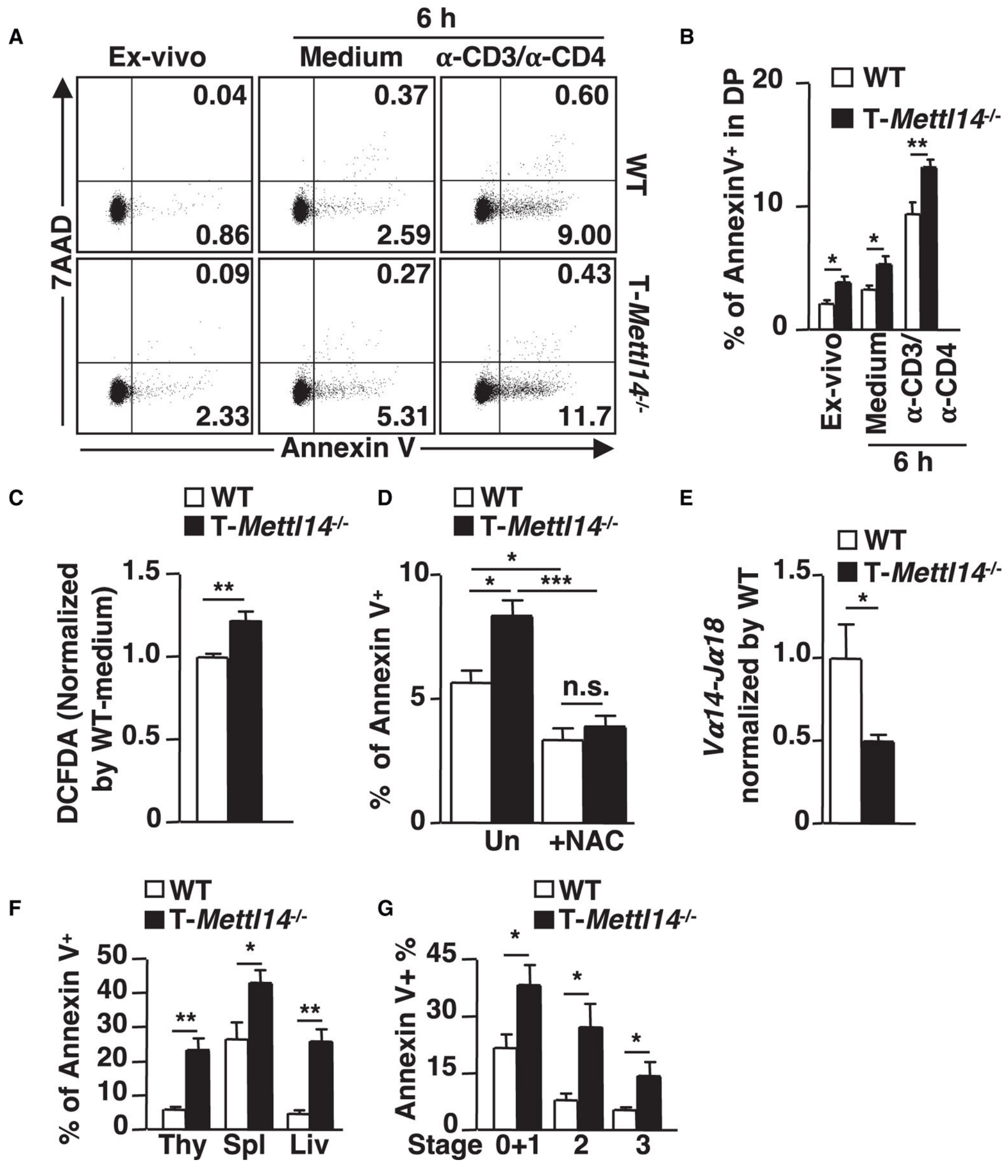

Figure 5. Elevated apoptosis in T-*Mettl14*$^{-/-}$ DP thymocytes is rescued by the scavenger of ROS

(A) Representative staining of apoptosis markers of naive and activated DP thymocytes.

(B) Percentage of Annexin V$^+$ cells in *ex vivo*, 6-h medium culture, or anti-CD3/anti-CD4-stimulated DP thymocytes from WT and T-*Mettl14*$^{-/-}$ mice (n = 5–6).

(C) Intracellular ROS in DP thymocytes detected by DCFDA (n = 5).

(D) Percentage of Annexin V$^+$ population in DP thymocytes after 6-h incubation with or without NAC (n = 5).

(E) Relative expression of *Vα14-Jα18* in DP thymocytes of T-*Mettl14*$^{-/-}$ mice (n = 5).

(F) Percentage of Annexin V$^+$ population of iNKT cells in WT and T-*Mettl14*$^{-/-}$ mice from thymus, spleen, and liver (n = 7).

(G) Percentage of Annexin V$^+$ population of iNKT thymocytes at different developmental stages (n = 7). SEM is shown. *p < 0.05, **p < 0.01, ***p < 0.001.

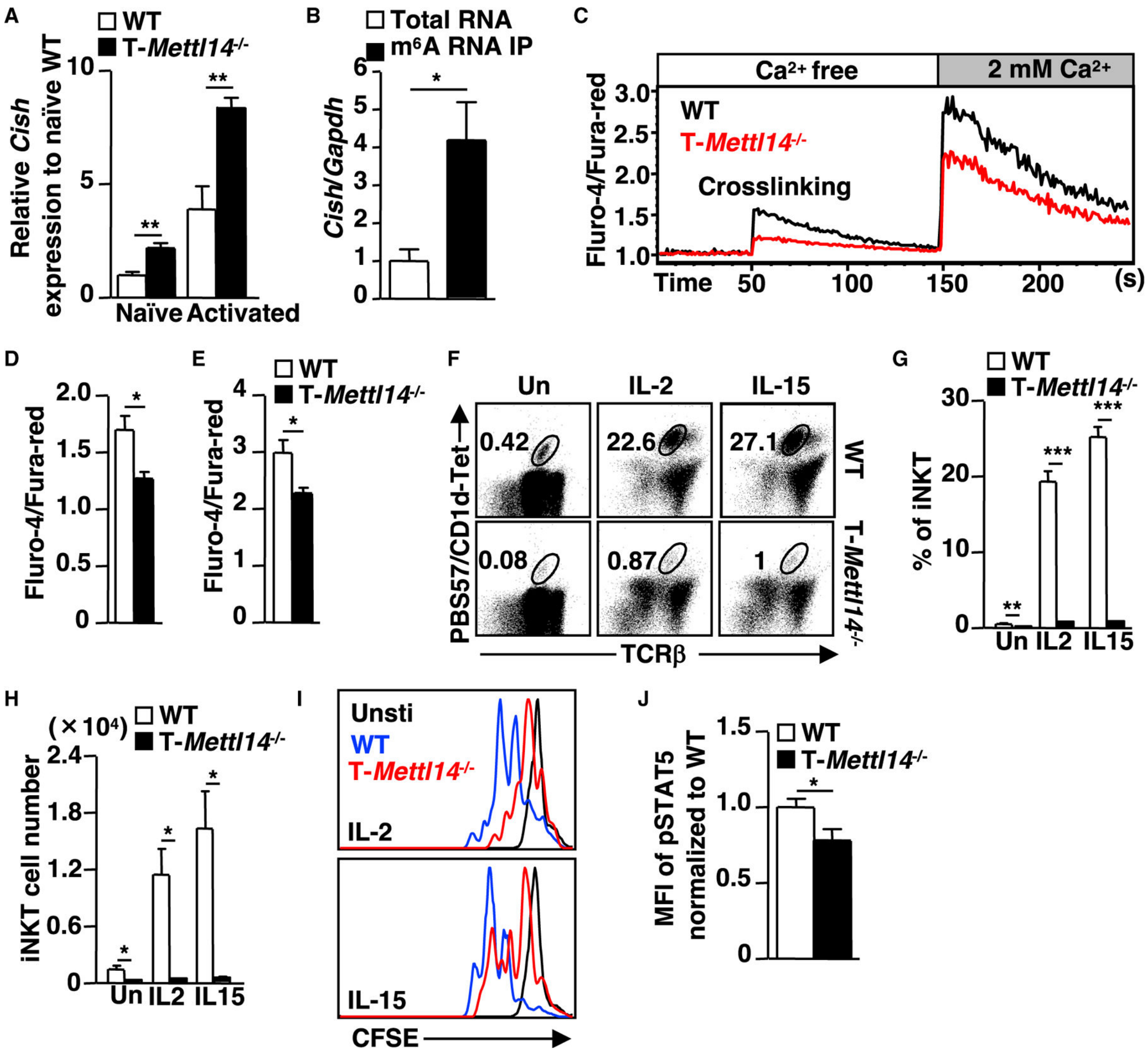

Figure 6. Upregulation of m^{6}A target gene *Cish* in *Mettl14*-deficient thymocytes correlates with decreased TCR signaling and impaired cytokine response

(A) Relative expression of *Cish* in naive and activated (anti-CD3/anti-CD4) DP thymocytes (n = 5–9).

(B) Relative expression of *Cish* in the m^{6}A RNA immunoprecipitation of total thymocytes RNA in WT mice by qPCR quantification (n = 4).

(C) Intracellular calcium flux in DP thymocytes in response to crosslinking of anti-CD3/anti-CD4 in T-*Mettl14*$^{-/-}$ mice.

(D and E) Quantification of maximum calcium flux on crosslinking and addition of Ca^{2+} in T-*Mettl14*$^{-/-}$ DP cells (n = 5–6).

(F) Representative staining of thymic iNKT cell expansion at day 3 after stimulation with IL-2 or IL-15.

(G and H) Percentage and cell number of thymic iNKT cells on D0 and D3 after stimulation with IL-2 or IL-15 (n = 5).

(I) Representative figure of cell trace distribution in thymic iNKT cells on day 3 post-stimulation with IL-2 or IL-15 (n = 5–6). Unstimulated thymocytes were used as controls.

(J) Bar graph of pSTAT5 in iNKT thymocytes after 20 min of IL-15 stimulation ($n = 5$). SEM is shown. *$p < 0.05$, **$p < 0.01$, ***$p < 0.001$.

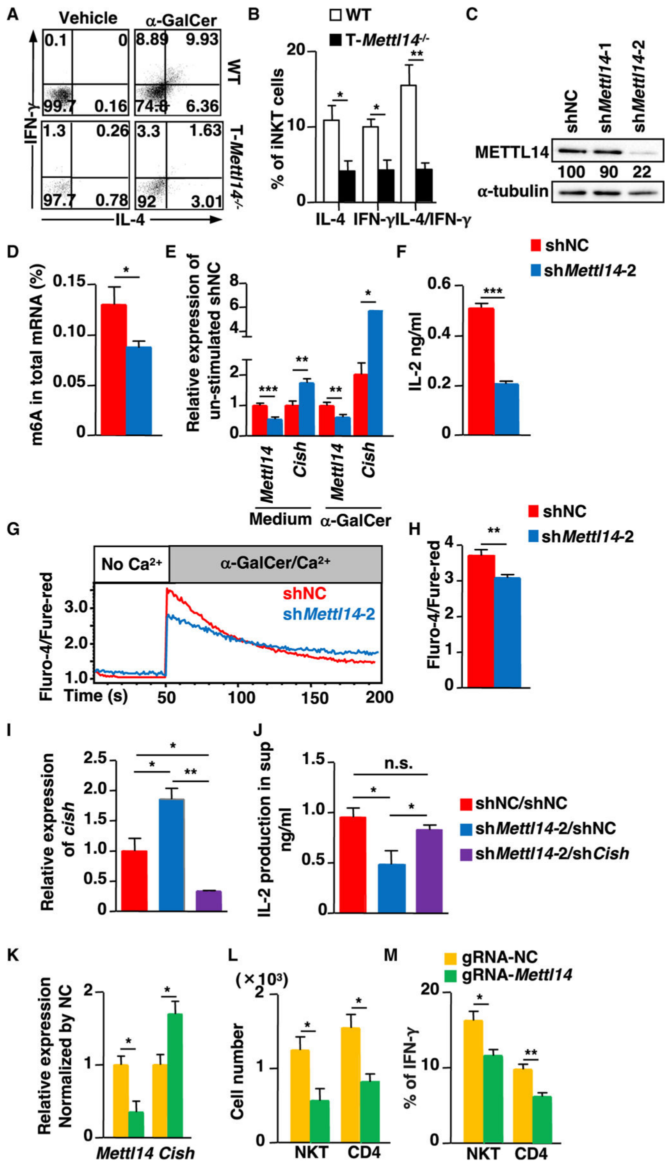

Figure 7. *Mettl14*-deficiency impairs mature iNKT cell function

(A) Dot plots of IFN-γ and IL-4 in residual iNKT cells from T-*Mettl14*$^{-/-}$ mice after *in vivo* *α*-GalCer stimulation.

(B) Quantification of the percentage of IFN-γ and IL-4 producing iNKT cells in α-GalCer-immunized WT and T-*Mettl14*$^{-/-}$ mice (n = 4).

(C) Expression of METTL14 in DN32.D3 cells transduced with lentivirus coding *Mettl14*-specific shRNA (sh*Mettl14*-1 or sh*Mettl14*-2) or control shRNA (shNC).

(D) m^{6}A level in mRNA of DN32.D3 cells transduced with sh*Mettl14*-2 and shNC.

(E) Relative expression of *Mettl14* and *Cish* in DN32.D3-sh*Mettl14*-2 in medium or stimulation with α-GalCer for 24 h.

(F) Production of IL-2 in DN32.D3-sh*Mettl14*-2 after stimulation with α-GalCer for 24 h quantified by ELISA.

(G) Intracellular calcium flux in DN32.D3-sh*Mettl14*-2 cells in response to α-GalCer/Ca^{2+}.

(H) Quantification of maximum calcium flux upon α-GalCer stimulation. Data representative of three to six independent experiments. shNC or sh*Mettl14*-2-treated DN32.D3 were spin-transduced with retrovirus carrying sh*Cish* or shNC. $Zsgreen^{+}$ cells were sorted and cultured.

(I) Relative expression of *Cish* in the indicated groups.

(J) IL-2 production in shNC/shNC-treated (''WT'' control) and shNC and shCish-treated $Mettl14^{KD}$ DN32.D3 cells after stimulation with α-GalCer for 24 h. $V\alpha14^{Tg}$ splenocytes were nucleofected with rCas9/gRNA complex and maintained in complete RPMI supplemented with IL-2 for 3 days.

(K) *Mettl14* and *Cish* expression by qPCR on day 3 after nucleofection.

(L) Absolute cell numbers of iNKT and $CD4^{+}$ T cells after nucleofection.

(M) IFN-γ production in iNKT and $CD4^{+}$ T cells after nucleofection ($n = 3–4$). SEM is shown. $*p < 0.05$, $**p < 0.01$, $***p < 0.001$.

KEY RESOURCES TABLE

REAGENT or RESOURCE	SOURCE	IDENTIFIER
Antibodies		
Biotin anti-mouse/human CD45R/B220 antibody	BioLegend	RRID: AB_312988
Biotin anti-mouse CD19 antibody	BioLegend	RRID: AB_313638
Biotin anti-mouse CD8α antibody	BioLegend	RRID: AB_312742
Biotin anti-mouse CD8β.2 antibody	BioLegend	RRID: AB_10641695
Biotin anti-mouse CD11b antibody	BioLegend	RRID: AB_312786
Biotin anti-mouse CD11c antibody	BioLegend	RRID: AB_313772
Biotin anti-mouse Ter-119/Erythroid cells antibody	BioLegend	RRID: AB_313704
Biotin anti-mouse I-A/I-E antibody	BioLegend	RRID: AB_313318
Biotin anti-mouse CD4 antibody	BioLegend	RRID: AB_2561504
Biotin rat anti-mouse IL-2	BD Biosciences	RRID: AB_395384
anti-mouse CD3ε antibody	BioXcell	RRID: AB_1107634
Purified rat anti-mouse IL-2	BD Biosciences	RRID: AB_395383
anti-Thy-1.2 (AT83.A-6)	Self-made	RRID: CVCL_9186
Rabbit anti-mouse METTL14 antibody	MilliporeSigma	RRID: AB_10672401
Rabbit anti-mouse METTL3/MT-A70 antibody	Proteintech	RRID: AB_2142033
Mouse anti-mouse α-tubulin antibody	Calbiochem	RRID: AB_2617116
m^{6}A-specific antibody	Synaptic Systems	RRID: AB_2279214
FITC anti-mouse CD1d	Self-made	(Mandal et al., 1998)
BV421 anti-mouse TCRβ antibody	BD Biosciences	RRID: AB_2737830
BV510 anti-mouse CD8α antibody	BD Biosciences	RRID: AB_2687548
PerCP anti-mouse CD4 antibody	BioLegend	RRID: AB_893331
PE anti-NK1.1 antibody	BioLegend	RRID: AB_313394
FITC anti-mouse CD24 antibody	BioLegend	RRID: AB_312838
PerCP anti-mouse CD69 antibody	BioLegend	RRID: AB_940497
PE-Cy7 anti-mouse/human CD44 antibody	BioLegend	RRID: AB_830786
PerCP anti-mouse F4/80 antibody	BioLegend	RRID: AB_893495
PerCP anti-mouse/human CD45R/B220 antibody	BioLegend	RRID: AB_893355
BV510 anti-mouse CD45.1 antibody	BioLegend	RRID: AB_2563378
PerCP anti-mouse CD45.2 antibody	BioLegend	RRID: AB_893351
PE anti-mouse EGR2 antibody	Thermo Fisher Scientific	RRID: AB_10717803
PE anti-mouse PLZF antibody	BioLegend	RRID: AB_2561966
PE-Cy7 anti-T-bet	BioLegend	RRID: AB_2561760
PerCP anti-mouse RORγt	BD Biosciences	RRID: AB_2737720
PE anti-mouse IL-4 antibody	BioLegend	RRID: AB_315317
FITC anti-mouse IFN-γ antibody	BioLegend	RRID: AB_315399
PE Rat IgG1, κ Isotype Ctrl antibody	BioLegend	RRID: AB_326513
FITC Rat IgG1, κ Isotype Ctrl Antibody	BioLegend	RRID: AB_326511
PE Mouse Anti-Stat5 (pY694)	BD Biosciences	RRID: AB_10894188
PE anti-mouse CD4	BioLegend	RRID: AB_312692

REAGENT or RESOURCE	SOURCE	IDENTIFIER
Bacterial and virus strains		
Lentivirus harboring shRNA targeting murine *Mettl14* (shNC, Mettl14-sh1 and sh2)	MilliporeSigma	Cat#: TRCN0000084996
Retrovirus harboring shRNA targeting murine *Cish and shNC*	TAKARA	Cat#: 632455
Stbl3™ *E. coli*	Thermo Fisher Scientific	C737303
Chemicals, peptides, and recombinant proteins		
PE-conjugated PBS57/mCD1d-tetramer	NIH Tetramer core facility	N/A
APC-conjugated PBS57/mCD1d-tetramer	NIH Tetramer core facility	N/A
PE-conjugated mCD1d unloaded tetramer	NIH Tetramer core facility	N/A
APC-conjugated mCD1d unloaded tetramer	NIH Tetramer core facility	N/A
PE 5-OP-RU MR1 tetramers	NIH Tetramer core facility	N/A
PE 6-FP-loaded MR1 tetramers	NIH Tetramer core facility	N/A
N^6-methyladenosine 5′-monophosphate sodium	MilliporeSigma	Cat#: M2780–10MG
FITC Annexin V	BioLegend	Cat#: 640905
7AAD	BD Biosciences	Cat#: 559925
Recombinant Murine IL-15	Peprotech	Cat#: 210–15
Recombinant murine IL-2	Peprotech	Cat#: 212–12
α-GalCer	MilliporeSigma	Cat#: 867000P
rabbit complement	Cedarlane Laboratories	Cat#: CL3051
CM-H2DCFDA	Thermo Fisher Scientific	Cat#: C6827
N-acetyl cysteine (NAC)	MilliporeSigma	Cat#: 38520–57-9
Fluro-4	Thermo Fisher Scientific	Cat#: F14201
Fura-red	Thermo Fisher Scientific	Cat#: F3020
*Bam*H I	NEB	Cat#: R0136S
*EcoR*I	NEB	Cat#: R0101S
Lipofectamine LTX	Thermo Fisher Scientific	Cat#: 15338100
TrueCut™ Cas9 Protein v2	Thermo Fisher Scientific	Cat#: A36498
Critical commercial assays		
TRIzol	Thermo Fisher Scientific	Cat#: 15596026
Qiagen RNAeasy® mini kit	Qiagen	Cat#: 74004
Dynabeads™ mRNA purification kit	Thermo Fisher Scientific	Cat#: 61006
Qubit™ RNA High Sensitivity (HS) Kits	Thermo Fisher Scientific	Q32852
Enzyme-linked immunosorbent assay	EPIGENTEK	Cat#: P-9005–96
Foxp3 Staining buffer set	Thermo Fisher Scientific	Cat#: 00–5523-00
Illumina Truseq preparation kit	Illumina	Cat#: RS-122–2001
Superscript III reverse transcriptase	Thermo Fisher Scientific	Cat#: 18080–044
PerfeCTa SYBR Green FastMix	Quantabio	Cat#: 95071–012
Protein G Dynabeads	Thermo Fisher Scientific	Cat#: 88847
Trizol LS	Thermo Fisher Scientific	Cat#: 10296010
CellTrace™ Violet cell proliferation Kit	Thermo Fisher Scientific	Cat#: C34557
P4 primary cell 4D-NucleofectorTM X Kit S	Lonza	Cat#: V4XP-4032
Deposited data		

REAGENT or RESOURCE	SOURCE	IDENTIFIER
Raw and processed file: RNA-Seq for DP thymocytes in T-*Mettl14*$^{-/-}$ mice	This paper	GSE189339
Experimental models: Cell lines		
iNKT cell hybridoma (DN32.D3)	(Bendelac, 1995; Lantz and Bendelac, 1994)	N/A
293T cells	ATCC	ATCC: CRL-3216
Phoenix-Eco	ATCC	ATCC: CRL-3214
J1j.10	ATCC	ATCC: TIB-184
Experimental models: Organisms/strains		
T-*Mettl14*$^{-/-}$ mice	(Lu et al., 2020)	N/A
C57BL/6J (B6) mice	Jackson Laboratory	JAX: 000664
C57BL/6-Tg(Cd4-TcraDN32D3)1Aben/J (Vα14Tg) mice	Jackson Laboratory	JAX: 014639
B6.SJL-Ptprca Pepcb/BoyJ (CD45.1) mice	Jackson Laboratory	JAX: 002014
Jα18$^{-/-}$ mice	(Cui et al., 1997)	N/A
Recombinant DNA		
pLKO.1	MilliporeSigma	Cat#: TRCN0000084996
pMD2.G	Addgene	Addgene: 12259
psPAX2	Addgene	Addgene: 12260
pSIREN-RetroQ-Zsgreen	Takara	Takara: 632455
pCL-Eco	Addgene	Addgene: 12371
Software and algorithms		
FlowJo 10	BD Biosciences	https://www.flowjo.com/solutions/flowjo/downloads/
Ceto pipeline (Trimmomatic, STAR, and HTseq)	(Anders et al., 2015; Bolger et al., 2014; Dobin et al., 2013)	https://github.com/ebartom/NGSbartom
DESeq2	(Love et al., 2014)	https://bioconductor.org/packages/release/bioc/html/DESeq2.html
GSEA	(Subramanian et al., 2005)	https://www.gsea-msigdb.org/gsea/index.jsp
GSEA	(Subramanian et al., 2005)	https://www.gsea-msigdb.org/gsea/index.jsp
Microsoft Excel	Microsoft	https://www.microsoft.com/en-us/microsoft-365/microsoft-office
GraphPad 6.0	GraphPad Software Inc	https://www.graphpad.com/
Oligonucleotides		
Vα14-Jα18 forward primer: TAAGCACAGCACGCTGCACAT	(Koseki et al., 1991)	N/A
Vα14-Jα18 reverse primer: CAATCAGCTGAGTCCCAGCT	(Koseki et al., 1991)	N/A
Cish forward primer: CTCTGGGACATGGTCCTTTG	(Li et al., 2017)	N/A
Cish reverse primer: GGCATCTTCTGTAGGTGCTG	(Li et al., 2017)	N/A
Socs1 forward primer: CGTCCTGCCGCCAGATGAG	(Li et al., 2017)	N/A
Socs1 reverse primer: GCCAACAGACCCCAAGGAG	(Li et al., 2017)	N/A

REAGENT or RESOURCE	SOURCE	IDENTIFIER
Socs2 forward primer: CTGCGCGAGCTCAGTCAAAC	(Li et al., 2017)	N/A
Socs2 reverse primer: GTCTGAATGCGAACTATCTC	(Li et al., 2017)	N/A
Socs3 forward primer: AGATTTCGCTTCGGGACTAG	(Li et al., 2017)	N/A
Socs3 reverse primer: GGAGCCAGCGTGGATCTGC	(Li et al., 2017)	N/A
Hmga1b forward primer: CAGCTCCAGGGAGGAAACC	(You et al., 2014)	N/A
Hmga1b reverse primer: AGGACTCCTGGGAGATGC	(You et al., 2014)	N/A
Mettl14 forward primer: CTGAGAGTGCGGATAGCATTG	(Cheng et al., 2021)	N/A
Mettl14 reverse primer: GAGCAGATGTATCATAGGAAGCC	(Cheng et al., 2021)	N/A
Gapdh forward primer: GTTGTCTCCTGCGACTTCA	(Prima et al., 2017)	N/A
Gapdh reverse primer: GGTGGTCCAGGGTTTCTTA	(Prima et al., 2017)	N/A
β-actin forward primer: CTTCTTTGCAGCTCCTTCGTT	(Heller et al., 2014)	N/A
β-actin reverse primer: AGGAGTCCTTCTGACCCATTC	(Heller et al., 2014)	N/A
Trim25 forward primer:	Bio-Rad	N/A
Trim25 reverse primer:	Bio-Rad	N/A
Xaf1 forward primer:	Bio-Rad	N/A
Xaf1 reverse primer:	Bio-Rad	N/A
shRNA for Mettl14-1: CCGGCTATGATACATCTGCTCCAAACTCGAGTTT GGAGCAGATGTATCATAGTTTTTG	MilliporeSigma	N/A
shRNA for Mettl14-2: CCGGGCATTGGTGCTGTGTTAAATACTCGAGTA TTTAACACAGCACCAATGCTTTTTG	MilliporeSigma	N/A
sh*Cish*: GATCCGGTACATTCCTAGTTCGAGATTCAAGAG ATCTCGAACTAGGAATGTACCTTTTTTG	(Funakoshi-Tago et al., 2017)	N/A
Other		
LB medium	Thermo Fisher Scientific	Cat#: 12780–052
RPMI 1640	CORNING	Cat#: 15–040-CV
FBS	PEAK serum	Cat#: PS-FB1
L-Glutamine 100*	Hyclone	Cat#: SH30034.01
HEPES	Hyclone	Cat#: SH3023701
2-Mercaptoethanol	Gibco	Cat#: 21985–023
Penicillin-Streptomycin (10,000 U/mL)	Hyclone	Cat#: SV30010
DPBS, no calcium, no magnesium	Thermo Fisher Scientific	Cat#: 14190250
DMEM media	CORNING	Cat#: 10–013-CV
anti-CD4 (L3T4) Microbeads	Miltenyi Biotec	Cat#: 130–117-043
anti-CD8α (Ly-2) Microbeads	Miltenyi Biotec	Cat#: 130–117-044
Dynabeads™ Biotin Binder	Thermo Fisher Scientific	Cat#: 11047
Bovine serum albumin (BSA)	MilliporeSigma	Cat#: A9418–500G
Paraformaldehyde (PFA)	MilliporeSigma	Cat#: P6148–500G
Saponin	poreSigma	Cat#: SAE0073–10G
Phosflow™ Fix Buffer I	BD	Cat#: 557870
Perm/Wash buffer™	BD	Cat#: 554723
Pharmingen™ Stain Buffer	BD	Cat#: 554657
Alkaline Phosphatase Streptavidin	Jackson Immunoresearch	Cat#: 016050084

REAGENT or RESOURCE	SOURCE	IDENTIFIER
Phosphatase substrate	MilliporeSigma	Cat#: S0942–200TAB
RNasin® Ribonuclease Inhibitors	Promega	Cat#: N261B
Monensin	AMRESCO	Cat#: K645–500mg
Puromycin dihydrochloride	MilliporeSigma	Cat#: P8833–10MG
Ficoll-Paque	MilliporeSigma	Cat#: GE17–1440-02